BMBF-Förderkennzeichen:

02MOST2019

BMBF-MOST-Kooperation:

Förderung wassertechnologischer F&E-Vorhaben im Rahmen der deutsch-israelischen Zusammenarbeit auf wissenschaftlich-technischem Gebiet

- Schlussbericht –

Fachliche und administrative Projektbetreuung:

Projektträger Karlsruhe
Wassertechnologie und Entsorgung (PTKA-WTE)
Karlsruher Institut für Technologie (KIT)

Zusammenstellung stellvertretend für das Ministry of Science and Technology, Israel (MOST)
Anika Sibler

Hinweis:

Die diesem Bericht zugrunde liegenden F&E-Vorhaben wurden mit Mitteln des Bundesministeriums für Bildung und Forschung (BMBF) und des Ministry of Science and Technology, Israel (MOST) unter dem Förderkennzeichen 02MOST2019 gefördert.

Die Verantwortung für den Inhalt dieser Veröffentlichung liegt bei den Autoren.

Berichtsblatt

1. ISBN oder ISSN	2. Berichtsart (Schlussbericht oder Veröffentlichung) **Schlussbericht**

3. Titel

BMBF-MOST-Kooperation:
Förderung wassertechnologischer F&E-Vorhaben im Rahmen der deutsch-israelischen Zusammenarbeit auf wissenschaftlich technischem Gebiet

4. Autor(en) [Name(n), Vorname(n)]	5. Abschlussdatum des Vorhabens
Prof. Dr. Avi Ostfeld[1] Daniel Mandler[2]	6. Veröffentlichungsdatum
	7. Form der Publikation **Schlussbericht**
8. Durchführende Institution(en) (Name, Adresse) Technion City[1] Hebrew University of Jerusalem[2]	9. Ber. Nr. Durchführende Institution
	10. Förderkennzeichen *) **02MOST2019**
	11. Seitenzahl
12. Fördernde Institution (Name, Adresse) Bundesministerium für Bildung und Forschung (BMBF) 53170 Bonn	13. Literaturangaben
	14. Tabellen
	15. Abbildungen

16. Zusätzliche Angaben

17. Vorgelegt bei (Titel, Ort, Datum)

18. Kurzfassung

Dieser Bericht umfasst die Einzelberichte der israelischen Forschungseinrichtungen über folgende Projekte, die im Rahmen der Wassertechnologie-Kooperation des Bundesministeriums für Bildung und Forschung (BMBF) und des Ministry of Science and Technology (MOST) gefördert wurden:

- MoDiCon: Online-Monitoring und digitale Steuerung in Trinkwasserversorgungssystemen (Projekt Nr. WT1901)

- NEMWARE: NanoElektroMembranverfahren zur Entfernung von Spurenschadstoffen bei der Wiederverwendung von Wässern (Projekt Nr. WT1902)

19. Schlagwörter
Abwasseraufbereitung, Entsalzung, Nanofiltration

20. Verlag	21. Preis

*) Auf das Förderkennzeichen des BMBF soll auch in der Veröffentlichung hingewiesen werden.

Document Control Sheet

1. ISBN or ISSN	2. type of document (e.g. report, publication) **Final Report**

3. title

BMBF-MOST-Kooperation:
Förderung wassertechnologischer F&E-Vorhaben im Rahmen der deutsch-israelischen Zusammenarbeit auf wissenschaftlich technischem Gebiet

4. author(s) (family name, first name(s))	5. end of project
Prof. Dr. Avi Ostfeld[1] Daniel Mandler[2]	6. publication date
	7. form of publication **Final Report**
8. performing organization(s) (name, address) Technion City[1] Hebrew University of Jerusalem[2]	9. originator's report no.
	10. reference no. **02MOST2019**
	11. no. of pages
12. sponsoring agency (name, address) Bundesministerium für Bildung und Forschung (BMBF) 53170 Bonn	13. no. of references
	14. no. of tables
	15. no. of figures

16. supplementary notes

17. presented at (title, place, date)

18. abstract

This report includes the individual reports of the Israeli research institutes of the following projects granted within the framework of the Water Technology Cooperation between the Federal Ministry of Education and Research (BMBF) and the Ministry of Science and Technology (MOST):

- MoDiCon: Online Monitoring and Digital Control in drinking water distribution systems (Project WT1901)
- NEMWARE: NanoElectroMembrane processes for micropollutant removal in WAter REuse (Project WT1902)

19. keywords

20. publisher	21. price

BMBF-MOST- Cooperation in Water Technology Research

Projects within agreement 02MOST2019

(Correlated projects are **framed bold**, the German partner's projects are ***italicized***)

Cooperation No.	Project No.	Topic	Research Institution (GER)	Principal Investigator (GER)	Research Institution (ISR)	Principal Investigator (ISR)	Period	BMBF-MOST-Grant [€]		
								Total	German partner	Israeli partner
1	WT1901	MoDiCon: Online Monitoring and Digital Control in drinking water distribution systems			Technion City	Prof. Dr. Avi Ostfeld		1.006.218,95		356.500,00 (89.125,00 MOST)
	02WIL1553 PT: Dr. L. Wolf	*MoDiCon: Online-Monitoring und digitale Steuerung in Trinkwasserversorgungssystemen*	*Universität Hamburg*	*Prof. Dr.-Ing. Mathias Ernst*					649718,95	
2	WT1902	NEMWARE: NanoElectroMembrane processes for micropollutant removal in WAter REuse			Hebrew University of Jerusalem	Daniel Mandler		704.123		256.450,00 (64.112,50 MOST)
	02WIL1555 PT: A. Sibler	*NEMWARE: NanoElektroMembranverfahren zur Entfernung von Spurenschadstoffen bei der Wiederverwendung von Wässern*	*KIT Karlsruhe*	*Prof. Dr. Andrea Schäfer*					*447673*	

WT1901
Online Monitoring and Digital Control in drinking water distribution systems

Federal Ministry of Education and Research (BMBF), Germany

Ministry of Science, Technology and Space (MOST), Israel

Joint German-Israeli Water Technology Research Program

JOINT FINAL REPORT

For the Period: 01.06.2020 until 30.09.2023

German Project Number: *02WIL1553A* Israeli Project Number: *3-17011*

Title of German Project: *Online-Monitoring und digitale Steuerung in Trinkwasserversorgungssystemen*

Title of Israeli Project: *Online Monitoring and Digital Control in Drinking Water Distribution Systems*

Israeli Principal Investigator -- including Institution and Department:
Professor Avi Ostfeld, Ph.D.
Insrael Insitute of Technoloogy – Technion,
Civil and Evironmental Engineering

German Principal Investigators -- including Institutions and Departments:
Professor Dr.-Ing. Mathias Ernst
Hamburg University of Technology
Institute of Water Resources and Water Supply

Professor Dr.-Ing. Pu Li
Ilmenau University of Technology
Institute for Automation and Systems Engineering

Signatures of

Israeli Principal Investigator: Date: 01.10.2023

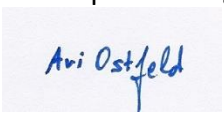

Prof. Avi Ostfeld, Ph.D.

German Principal Investigators: Date: 01.10.2023

Prof. Dr.Ing. Mathias Ernst

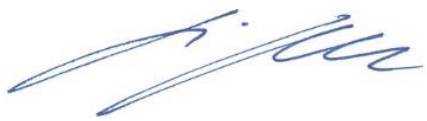

Prof. Dr.Ing. Pu Li

1. SCIENTIFIC OR TECHNICAL RESULTS

Abstract

The current digital transformation in the drinking water sector allows new processes of autonomous drinking water quality control processes for water distribution networks. Within the BMBF-MOST MoDiCon project, the consortium developed an integrated framework for simultaneous monitoring (i), simulating water quality parameters in a water distribution system (WDS) (ii) as well as taking automatic control actions (iii). The realization of this integrated framework required intensive lab- and pilot testing for microbial and organic water quality (TUHH), model development for predicting the water quality at each point of the WDS (Technion), and programming of automated risk mitigation algorithms (TU Ilmenau) to avoid harm at end-users' service points.

The innovative sensor system for real-time monitoring of microbial and organic parameters was coupled combining flow cytometry and fluorescence spectroscopy. It allows the generation of individual real-time fingerprints and thus rapidly detects water quality changes in the water matrices (<15 min). For this, the sensor system was adapted and calibrated in a labor batch setup before implementing it into a real pilot plant system at a water work side. The pilot plant system enabled the successful validation of the water fingerprinting approach under real flowing conditions. Associated partners Hamburg Wasser and sensor experts bbe moldenke supported this realization with hardware and technical expertise. In this regard, automation monitoring includes sampling, measuring, data analysis, and visualization. The development of an automatized PARAFAC (parallel factor analysis) model in particular, enables a detailed characterization of present organic matter. The automation code of the monitoring method is an important project outcome and will be made available by GitHup infrastructure as open-access software shortly after the project ends. The visualization part in particular gives an idea of what future digitalized drinking water quality monitoring will look like. Regarding reliable drinking water quality analysis model predictions require an accurate interpretation of hydrodynamics and the uncertainties associated with the multifaceted exchanges within the distribution pipes. However, knowledge about most exchanges within the WDS still needs to be improved. Therefore, state-of-the-art models exist merely as theoretical frameworks to understand the cause-effects of microbiological quality fluctuations in WDS and lack general applicability. Advancing the applicability and reliability of the mechanistic models necessitates adequate consideration of epistemic and aleatory uncertainties. In this interest, physical models (within a novel computer package named EPANET-C) were developed to realize the complexity that needs to be integrated into the modeling framework to describe the water quality dynamics in a real-world WDS accurately. Via built-in and customizable conceptual and mathematical models' directories, EPANET-C simplified WDS water quality modeling for users, even those lacking programming expertise. Under the test conditions considered, the simplest single-phase models were found to make microbiological quality predictions like the relatively complicated two-phase models. The study signified that the knowledge uncertainty (primarily associated with data paucity) associated with mechanisms concerning heterotrophic bacterial regrowth at the bulk phase and biofilm detachment at the wall phase is critical in controlling the reliability of the water quality models. Due to the flexibility, EPANET-C can become a de facto standard

tool in WDS quality modeling study both for industry and academia. Either monitored or predicted water quality changes (contamination) needed investigations in an optimized control strategy framework to isolate and remove the contaminant appropriately. In the first step, a model-based optimal control strategy was developed to address the contamination mitigation problem with special consideration of different hydraulic and water management parameters. For this model, the mass and energy conservation laws were used to describe the hydraulic properties of the WDS, and a one-dimensional advective transport model was simplified to describe the decay of chlorine in the pipelines. As a result, a nonlinear programming (NLP) optimization problem is formulated and solved to achieve the specified chlorine concentration, simulations are also performed. Based on this nonlinear model, a new mixed-integer nonlinear programming (MINLP) was developed to define the optimal position of isolation valves and control strategies after contamination in the WDS to separate the contaminants and reduce their impact. The flushing process was implemented on the established EPANET model of the Hamburg Wasser pilot plant. As a hypothesis, contamination was fed into the WDS from different locations in different scenarios, whereupon the hydraulic components were controlled within an optimal control strategy so that the contaminant was successfully separated and flushed out of the pipeline and the WDS could recover from the abnormal situation.

The collaborated partners of the MoDiCon project compiled a novel approach for a future fully automized drinking water quality monitoring and prediction system. The developed interface between physical monitoring and simulation and optimization tools is innovative and may help water suppliers to guarantee their WDS safety. However, the final application requires a long-term test phase of the MoDiCon approach in a real WDS.

Body of report

In the last two decades over 70 cases of contaminated drinking water with harmful impacts on consumers' health were reported (Efstratiou et al., 2017; Moreira & Bondelind, 2017). All cases could be related to bacteria spreading into the WDS, with various origins of the contamination entering the system. The rapid detection as well as the reaction to the contaminant failed or were not able due to missing online monitoring systems, respectively. Scenarios like this are expected to increase in the future because of several reasons. Climate change and its secondary effects might deteriorate the drinking water quality (i), natural disasters like heavy rainfall or floods can overflow and contaminate water reservoirs and tanks (ii). Furthermore, aging infrastructure can lead to pipe damage and associated occurrence of contamination (iii). Last, human errors or cyber- and physical attacks may infiltrate the system and have to be avoided (iv). That is where the MoDiCon idea starts about what future digitalized water supply and water supply security could be like. Aiming for the assurance of drinking water quality all over the WDS via automized methods requires different actions:

1. **Autonomous water quality monitoring systems at several locations in the WDS**
   Minimizing the consumers' risks in case of contamination requires the determination of the optimum location for monitoring systems. These monitoring systems must be able to rapidly detect even little changes in the water matrix considering organic and

microbial content. In case of a water quality change, the monitoring systems must communicate with controlling mechanisms.

2. **Predictions for water quality all over the WDS**
   Since actual measuring of the water quality is not feasible at any time and at any location in the network, advanced water quality simulating tools are required to predict the water quality for every part of the WDS. Further data-driven algorithms must be developed and trained to recognize water quality anomalies even before they appear in the monitoring systems
3. **Reaction and control in case of a contamination**
   To react appropriately in case of a contamination, optimum control strategies in terms of closing valves, and flushing the system must be developed. This requires the optimal location of automatic control instruments like vales in the WDS.

Aiming a solution for this pictured "Future WDS" needs expertise in different fields which can ideally be served by the three research groups TUHH, Technion, and TUIL. Within the MoDiCon project, the research groups developed some individual approaches and objectives to achieve the above points. The research results of each group are highlighted in the following subsections.

TUHH

Jonas Schuster and Mathias Ernst

In the following, the contribution of the TUHH research group to the overall MoDiCon project is presented. For this purpose, it is subdivided into the three main work packages that were essential for the successful implementation of the project.

WP1: Further development of a Flow Cytometry and Fluorescence Spectroscopy (EEM) data analysis (EEM based on PARAFAC), and generating real water quality database
WP2: Developing a laboratory environment for continuous and autonomous real-time (<15min) measurement
WP3: Application of developed methods in a pilot plant setup

WP1: Further development of Flow Cytometry and Fluorescence Spectroscopy (PARAFAC) data analysis, and generating real water quality database

Both methods, flow cytometry, and fluorescence spectroscopy, are not part of either German or Israeli standard operation procedures in drinking water quality analysis, although they find application in several other research fields (medicine, biochemistry, etc.). The transmission of continuous monitoring methods into a real environment for a water supplier such as Hamburg Wasser requires standard handling procedures as well as an added value to state-of-the-art methods. Therefore, the initial step was to characterize measuring range, sensitivity limits, etc.

Flow Cytometry

By the start of the MoDiCon project, TUHH acquired and installed a new flow cytometer (Cube 6 – Sysmex) with an additive automation unit (OC300 – onCyt). Flow cytometric parameters that play a role in the MoDiCon project are Total cell count (TCC), high nucleic acid cells (HNA), low nucleic acid cells (LNA), viable cells, and dead cells. These parameters were analyzed by following steps: Adding up to two fluorescent dyes (SYBR Green I and Propidium Iodide) to the water samples, incubating the samples (13 min), and analyzing them with the flow cytometer. Within the first experiments, the detection range of cells was successfully defined considering cells with different sizes, viable/dead, as well as different cell concentrations. Test series were performed with solutions containing isolated bacteria (*Escherichia coli*, 1 – 6 µm, and *Brevundimonas diminuta*, 0.3 – 2 µm), drinking- and groundwater samples from different Hamburg Wasser utilities. A detailed Python-based data analysis tool was developed using the open-source software FlowKit (White et al., 2021).

Fluorescence Spectroscopy

Natural water samples generally contain fluorophores as part of the natural organic matter, which all types of natural waters obtain. Fluorescence spectroscopy can detect and quantify these fluorophores. It is known as a robust method for rapid organic characterization, although the quantification of qualification of fluorophores and its influence on the microbiological environment in the water is still under research. An innovative approach to standardize the data evaluation is the parallel factor analysis (PARAFAC), whose research impact increased recently regarding natural water characterization (Murphy et al., 2013). PARAFAC is a mathematical decomposition tool that enables the subdivision of total fluorescent organic matter signals. The goal of the MoDiCon project was to further develop the PARAFAC method into a standardized automatic procedure that can be established for continuous monitoring of fluorescent organic matter in drinking water. The PARAFAC model which was developed during the project can distinguish the total fluorescent signal in between five and seven different organic components, standing for several types of fluorophores. Figure 1 shows the excitation and emission matrix (EEM) of all (here: six) decomposed organic components. Each water sample can thus be analyzed by PARAFAC for the intensity of these six components providing an individual organic fingerprint. The unique character of the developed six-component PARAFAC model was successfully applied to all investigated natural water samples (drinking water, wastewater, rainwater).

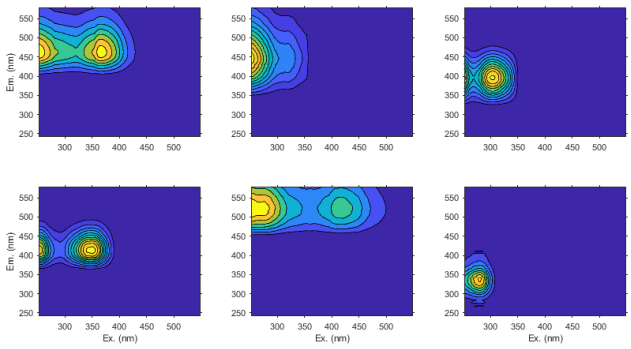

Figure 1: Developed six-component (C1 – C6 from top left to bottom right) PARAFAC model, validated for all kinds of investigated water samples. The peak excitation and emission wavelengths for each component are C1 λ_{ex} = 250/370 nm and λ_{em} = 465 nm, C2 λ_{ex} = 250/325 nm and λ_{em} = 450 nm, C3 λ_{ex} = 250/305 nm and λ_{em} = 400 nm, C4 λ_{ex} = 250/350 nm and λ_{em} = 420 nm, C5 λ_{ex} = 250/275/420 nm and λ_{em} = 525 nm, C6 λ_{ex} = 280 nm and λ_{em} = 335 nm.

By combining both techniques, the TUHH group generated individual microbial and organic fingerprints for different waters. An insight into these data is given in Table 1 for some chosen water samples.

Table 1: Overview of microbial and organic parameters from a few different natural water bodies. PARAFAC components based on the model (introduced in Figure 1).

Water body	Flow Cytometry			Organics	PARAFAC components					
	TCC	HNA	LNA	TOC	C1	C2	C3	C4	C5	C6
	in cells/mL			in mg/L	Fluorescence score in R.U.					
Drinking water 1	1.4×10^5	0.9×10^5	0.5×10^5	4.6	0.61	0.78	0.89	0.66	0.21	0.21
Drinking water 2	8.2×10^5	1.7×10^5	6.5×10^5	3.1	0.47	0.58	0.54	0.41	0.19	0.21
Wastewater	1.7×10^7	0.5×10^7	1.2×10^7	16.3	5.03	0.00	4.84	3.67	2.08	2.19
Rainwater	1.0×10^7	9.5×10^6	0.5×10^6	2.5	0.44	0.42	0.42	0.31	0.18	0.34

However, even little changes in the water matrices can influence the harmlessness of the drinking water quality. The detection of these little changes via continuous monitoring was part of the second and third work packages.

Another part of the first work package was the generating of bacteria growth rates which were needed for water quality simulation tools (Technion). The growth behavior of different drinking water bodies microorganisms was analyzed via online flow cytometry and maximum growth rates were calculated. These results are shown in the WP1 of the Technion group.

WP2: Developing a laboratory environment for continuous and autonomous real-time (<15min) measurement

Regarding a standardized application of monitoring microbial and organic fingerprints WDS via flow cytometry and fluorescence spectroscopy, an automated process was needed. This process includes 1. sampling, 2. pre-treatment, 3. measuring, 4. data analysis, and 5. visualization. Whereas the installed flow cytometric devices include steps 1. – 3., the entire process was developed for fluorescence spectroscopy (Figure 2). Time-limiting steps are the pre-treatment step of flow cytometry (13 minutes of dye incubation), as well as the fluorescence measurement and PARAFAC modeling, each takes approximately 7 minutes. Thus, the total duration of the automatic procedure for one sample, from sampling to visualization, was minimized to approximately 15 minutes which can be described as real-time regarding conventional microbiological drinking water investigations that require days of responses. However, this fact must be considered as limiting for the MoDiCon approach of autonomous reaction in case of a WDS contamination (TUIL).

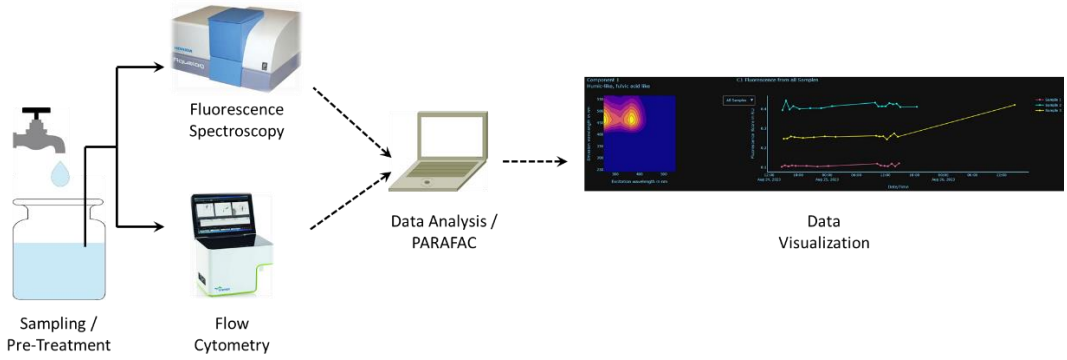

Figure 2: Schematic overview of automatic water quality monitoring on a lab scale. Data visualization shows an example of monitoring one PARAFAC component.

Besides the physical development of an automation unit for fluorescence spectroscopy, a very challenging part was the automation of PARAFAC data analysis in combination with data postprocessing. PARAFAC modeling was performed in MATLAB (version R2021b) using drEEM (version 0.6.5) toolbox, implementing little adjustments. For visualizing the PARAFAC data, the TUHH group developed a Python-based dashboard solution that also shows flow cytometric results. Furthermore, it is flexible for adding more real-time data from other devices (e.g., conductivity, turbidity, UV absorption, etc.). The real-time setup was successfully tested and experimental data was published in Schuster et al. (2022). Figure 3 shows some correlations that were investigated between organic matter and bacterial growth behavior.

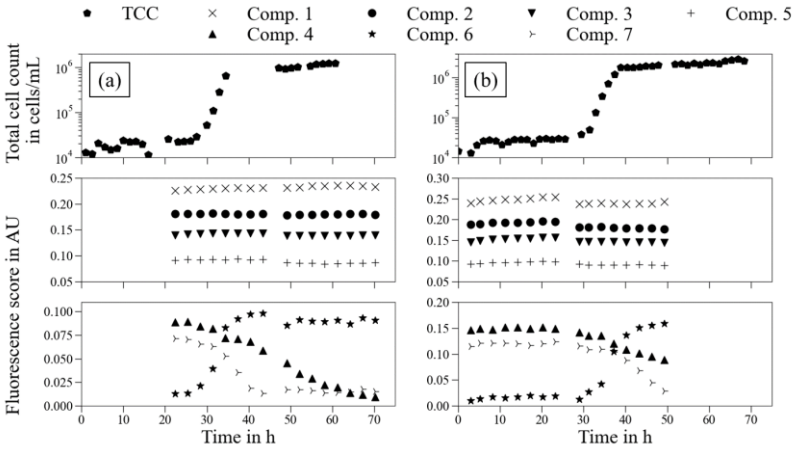

Figure 3: Experimental results from drinking water real-time monitoring via fluorescence spectroscopy (PARAFAC components 1- 7) and flow cytometry (Total cell count – TCC). The drinking water was spiked with organic nutrients to observe cell behavior in the presence of nutrients. Figure from Schuster et al., 2022.

The overall objective of this part was the development of a reliable and comparable method that can be adopted into WDS quality monitoring. For the introduced method, it is important to understand that it does not work with absolute limit values. Instead, it is necessary to generate water individual baseline values for all fluorescence components and flow cytometric parameters, respectively. Considering continuous monitoring, this approach detects even little discrepancies from the baseline values. Due to the type of changing fluorescence component / flow cytometric parameter and its intensity, it may be possible to identify the origin of the contamination and its criticality (e.g., sewage contamination and its amount). Due to the automated process, any critical changes can be reported immediately to the optimized control system (TUIL). Another offline application of this method is the building of a database for several wells or water work exits. The rapidity of the methods allows total monitoring over a long period, even for larger water suppliers such as Hamburg Wasser. Since defining water-specific limit values is one of the future key challenges of applying these methods to a real WDS, the next work package describes an initial approach for the implementation.

WP3: Application of developed methods into a pilot plant setup

In collaboration with Hamburg Wasser, the developed system was tested in a pilot plant flowing system. This pilot plant can simulate flow circumstances similar to the one in a real WDS. The pipe system, filled with approximately 4 m^3 of local drinking water (TCC = $1 - 2 \times 10^5$ cells/mL, TOC = 2.4 – 4.8 mg/L), flows in a circular closed loop with approximately 150 m length. With the adjusted volumetric flow rate of around 60 L/min, one round of the flowing water in the pilot plant took approximately 75 min. Under these stable conditions, small amounts (1 v%) of different natural waters (“contaminants”) were injected into the system. Table 1 contains an overview of the cell count (TCC) and total organic carbon (TOC) of the injected waters.

The objectives of the injection experiments were both, defining sensitivity limits of the methods in a flowing system and finding a way to characterize the injected water regarding its origin and potential hazardous components or general cases of contamination. To

perform these experiments, the pilot plant had to be adapted (sampling points, new pipes for closed loop, injection point, etc.). Figure 4 shows a flow chart sketch of the final pilot plant version.

Figure 4: Picture (a) from the indoor part and total flow chart sketch (b) of the Hamburg Wasser pilot plant.

The water quality of the system water was continuously monitored at the first sampling point (S1), located approximately 10 m (approximately 7 min under corresponding flow conditions) behind the injection point. The developed approach of simultaneous flow cytometric and fluorescence spectroscopic PARAFAC analysis (WP 2) was applied to these experiments as well. The monitoring of both was proven powerful in detecting little changes in drinking water. In combination, neither a microbiological change nor a change in organic matter content can be missed. Some exemplary results of the rainwater and wastewater injection experiments are shown in Figure 5. Both experiments simulated kind of contamination scenarios in a pipe system.

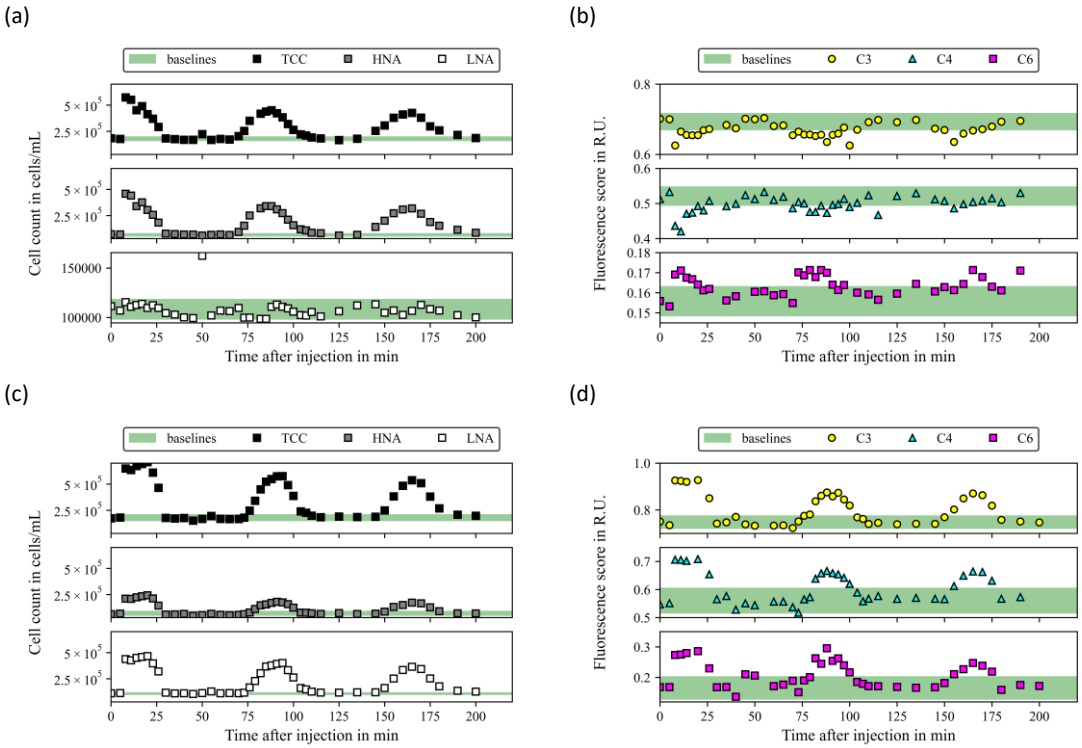

Figure 5: Particular monitoring results of the injection experiments. Cell count (TCC, HNA, and LNA) over time (a, and c), as well as the fluorescence score of three selected PARAFAC components (b, and d). The injected waters had their origin in collected rainwater (a, and b), and treated wastewater (c, and d).

All results show a significant deviation from the pilot plant baselines after approximately 7, 75, and 150 minutes. This correlates with the time duration needed for the water to pass the

sampling point (S1) and for the flow circulation two times afterward. Thus, it was possible to detect a little change in the water matrix which was enforced by injecting another type of water into the system. The microbial cell count of both injected waters was higher (> 1.0×10^7 cells/mL) than in the pilot plant water (approximately 2×10^5 cells/mL). However, they differ in the distribution of HNA and LNA cells (see Table 1). Rainwater was dominated by HNA cells, whereas wastewater was by LNA cells. This differentiation is shown by the monitoring results in (a) and (c). It explains how flow cytometric fingerprinting can not only detect contamination but also characterize it. The same was proven for fluorescence spectroscopic PARAFAC analysis. The lower amount of organic matter in rainwater -compared to the pilot plant- results in a reduction of the fluorescence score for C3 and C4 (b). In contrast to this, C6 showed a different behavior for all experiments. This component stands for protein-like organic compounds, and could slightly be correlated to TCC for all experiments. However, it does not show as high sensitivity as the determination of TCC by the flow cytometry. For a higher amount of organic matter in wastewater, all three components show an increase in the fluorescence score in the expected region (d).

The successful performance of this work package is fundamental when it comes to future application in a real WDS. Flow cytometry and Fluorescence spectroscopy including PARAFAC modeling can generate a unique microbial and organic fingerprint of a flowing system. Achieving baseline limit values for parameters, such as TCC, HNA, LNA, and PARAFAC components is significant for detecting critical deviations. In case of an unexpected event/increase/decrease of some parameters, the information must be transferred to the controlled system and the respective reaction will be launched (TUIL). TCC in particular can be used for continuous simulation for predicting the microbial load all over the WDS (Technion).

Technion

Gopinathan R. Abhijith, Leonid Kadinski, and Avi Ostfeld

The efforts of the Technion working group in the project consisted of four working packages. They are explained in detail below:

WP1: Interface between simulations and experiments:

The chosen model by Zhang et al. (2004) was adjusted for MoDiCon by excluding the chlorine compounds from the water quality simulation. The simulations were conducted using EPANET 2.0, including a MATLAB Toolkit for EPANET toolkit (Eliades et al. 2016) via MATLAB 2020a. The simulated main compounds included the mass concentration or total cell count (TCC) of bacteria in the drinking water as well as the substrate concentration utilized for bacterial growth. The model of Zhang (2004) uses a simple Monod kinetics approach where the growth rate of bacteria can be determined, as seen in (1), and the concentration of the substrate is expressed in (2).

$$\frac{\mathrm{dX}}{\mathrm{dt}} = \mu \cdot X \qquad (1)$$

$$\frac{\mathrm{dS}}{\mathrm{dt}} = \frac{\mu \cdot X}{Y} \quad (2)$$

Where X is the total count of bacterial cells and S is the concentration of the substrate. In the specific case of the model in Zhang et al. (2004), S represents the biodegradable fraction of dissolved organic carbon (BDOC, dissolved organic carbon: DOC), Y is the growth yield coefficient of bacteria, and μ is the specific growth coefficient. While the model used biodegradable organic carbon (BDOC) as the substrate to model bacterial growth, the challenge for this WP was to simulate parameters that can be validated in online measurements with flow cytometry and fluorescence spectroscopy. The first measurements by the laboratory in the TUHH indicated bacterial growth behavior and the respective DOC. As only a fraction of DOC can be utilized by bacteria as an energy source for growth (Prest et al. 2016), the sole measurement of DOC cannot be used to validate the conducted simulations. Assimilable Organic Carbon (AOC) is a parameter that describes the fraction of easily accessible carbon for present bacteria in drinking water. It is a maximum of up to 5% of DOC. For drinking water analysis, the AOC parameter is more convenient than BDOC. Hammes and Egli (2005) introduced a methodology to determine AOC using flow cytometry where bacteria concentration is observed over several days. To initialize the water quality simulations, the dependency of the specific growth coefficient to the substrate is required, which the bacteria use for growth for correctly modeling regrowth in the WDS model. This specific bacterial growth coefficient μ can be calculated as follows:

$$\mu = \frac{\mu_{max}}{S + K_s} \quad (3)$$

Where μ_{max} is the maximum bacterial growth rate respective to utilized substrate and K_s, the half-saturation constant, is the substrate at $\mu_{max}/2$.

To retrieve the specific growth rate that corresponds to the laboratory experiments of the TUHH, the maximum growth rate of various bacterial growth rate experiment series was plotted over the respective initial substrate concentration as seen in Figure 6. The substrate for these experiments was determined to be AOC. Each data point stands for one growth experiment. To calculate the specific growth rate μ with equation (3), a non-linear parameter estimation was conducted with the conducted. From these data μ_{max} was determined, as well as K_s.

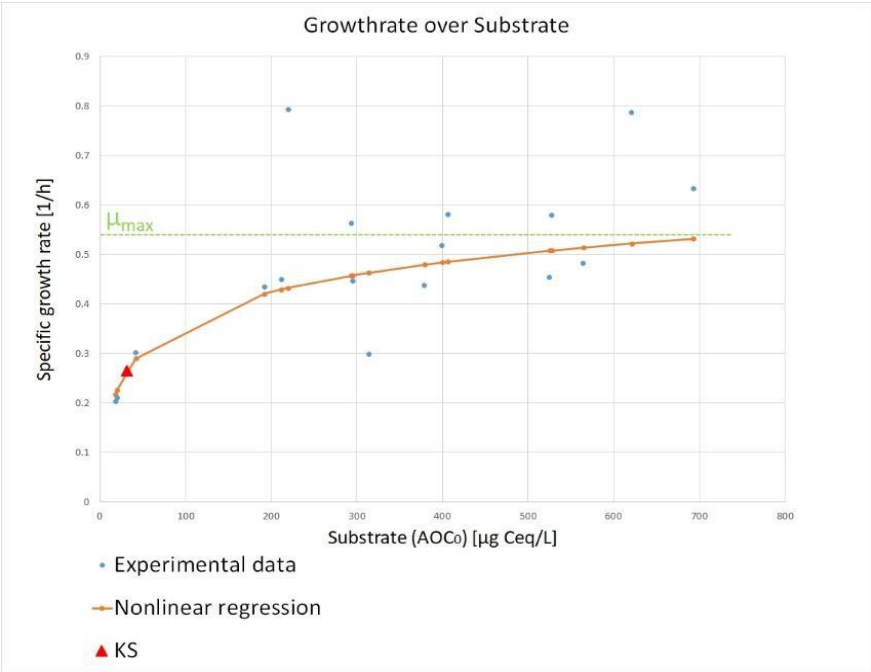

Figure 6: Maximum bacterial growth rate plotted over respective initial substrate concentration (AOC) from 17 experiment series. The non-linear regression was used to determine the parameters for the specific bacterial growth rate.

The calculated values were used for the first simple water quality simulation, which is described below. Monod kinetics was used to model the bacterial growth in the water network inside the simulation tool EPANET-MSX. The various equation coefficients were taken from the laboratory experiment evaluation of the TUHH. The WDS model chosen is the EPANET Net3 network. This study places fixed water quality sensors at nodes 159, 113, 184, 173, and 211, as seen in Figure 7. The presented scenario considers a substrate/organics injection at three network sources (see Figure 7). A minimal specific global level of bacteria in the system must be defined; otherwise, the equilibrium equations cannot be solved. The simulation time was 24 hours, and the duration of the substrate injection in scenarios 1 and 2 was 6 hours from the beginning of the simulation. The substrate concentration, which was injected, was 300 µg/L per minute.

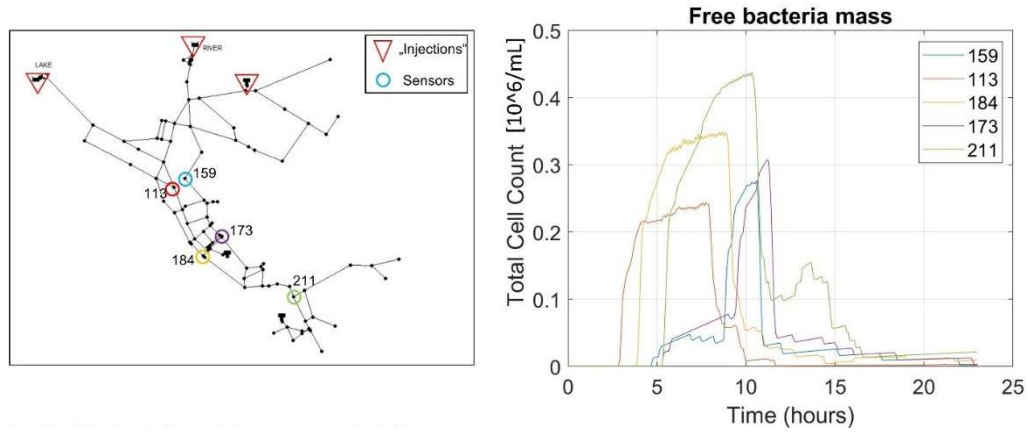

Figure 7: Example scenario simulated applying the bacterial regrowth model.

After establishing the interface between the laboratory experiments and the water quality simulations, the overarching goal was to validate the model through a sensitivity analysis using flow experiments. After the validation, the model was fused with deepened simulations (see WP-2) and expanded continuously.

WP2: Deepened, complex water quality simulations with chemical and biological compounds.

The tasks completed for WP-2 involved a comprehensive review of relevant literature pertaining to chemical and biological water quality parameters in WDS, building an environment (EPANET-C) for performing flow and transport simulations of relevant water quality parameters, and conducting deepened simulations in drinking WDS. EPANET-C is designed to be an advanced open-source extension of EPANET–EPANET-MSX modeling. It uses function directories to integrate the necessary resources for implementing multi-species reactive-transport (MSRT) models via the well-established EPANET–EPANET-MSX framework.

EPANET-C incorporates fifteen multi-species reactive-transport (MSRT) modules, each integrating the transport (via advection) and exchanges (physical, chemical, physicochemical, and biochemical reactions) of different combinations of the eleven reacting constituents i.e., nine abiotic constituents – chlorine, total organic carbon (TOC), biodegradable dissolved organic carbon (BDOC), trihalomethanes (THMs), 2,4,6-trichlorophenol (2,4,6-TCP), 2,4,6-trichloroanisole (2,4,6-TCA), perfluorooctaneamido betaine (PFOAB), perfluorooctaneamido ammonium salt (PFOAAmS), and perfluorooctanoic acid (PFOA) – and two biotic constituents – planktonic and biofilm microorganisms. The scientific information reported in our works was comprehended to establish the theoretical backgrounds of these modules. The conceptual model graphic of the comprehensive EPANET-C module (named 1234) is illustrated in Figure 8.

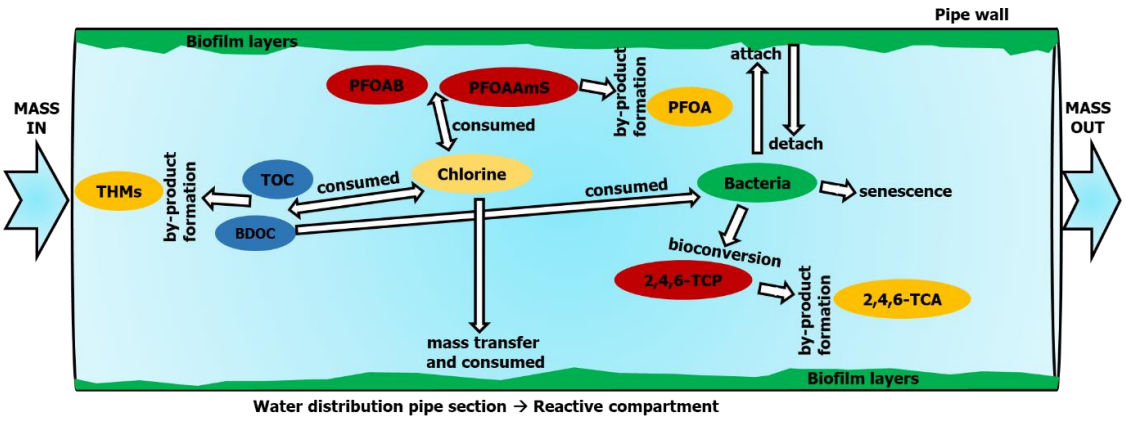

Figure 8: Conceptual framework of EPANET-C MSRT Module 1234.

EPANET-C is developed to be used as a shared object library. Thus, the programming interface of MATLAB was utilized for its calling and for water quality model implementation. However, to make the programming necessities in MATLAB more effortless or altogether bypass the same, the EPANET-C function directories were devised and operated. These in-built function directories of EPANET-C comprise every information concerning the MSRT

modeling. This includes the type and number of reacting constituents, conceptual information about the multi-species reactions, values of reaction rate coefficients, and the governing equations for all the contamination events simulated by applying EPANET-C.

Presently, EPANET-C is developed to function as an advanced extension of EPANET – EPANET-MSX modeling. A MATLAB (not older than the 2017b version) interface was created to attain this. The EPANET-C–MATLAB interface facilitates the loading and opening of the EPANET-C function libraries, provides input information, and implements hydraulic and water quality modeling. The hydraulic modeling and water quality modeling, precisely MSRT modeling, are executed using the EPANET and EPANET-MSX dynamic link libraries (DLL) for Windows. The EPANET-MATLAB toolkit was employed in this direction to utilize the EPANET and EPANET-MSX DLL. In total, the EPANET-C–MATLAB interface integrates the internal functions to make direct calls to the EPANET-MATLAB toolkit and performs MSRT modeling of WDS.

WP3: Data-driven event detection algorithms

A brief overview of the second work package, which deals with training machine learning algorithms with real-life water quality data to determine possible water quality anomalies, is given below. Recent studies have used machine learning methodologies to detect water quality anomalies and their sources by training these algorithms with specific water quality parameters as input features to predict possible water events. Artificial and convolutional neural networks (ANN/CNN) and support vector machines (SVM) have been used to detect whether a contamination event has occurred in a water network (Asheri et al., 2019; Ashwini et al., 2019). MoDiCon´s associate partner, Hamburg Wasser, the water utility of Hamburg, provided the project with a significant amount of water quality data for five years. The data from 22 sampling points in 19 waterworks was pre-processed and analyzed with various data evaluation packages in Python. The overarching goal was to train an ANN and a random forest algorithm with parameters that can be measured online to determine whether there is an anomaly in the water network. Figure 9 shows a conceptual layout of an ANN where the respective data for the input and output layer of the neural network is shown. The overarching goal was to create a support tool for water utilities to explore water quality online and in real-time and understand whether additional laboratory check-ups of the water quality need to be conducted.

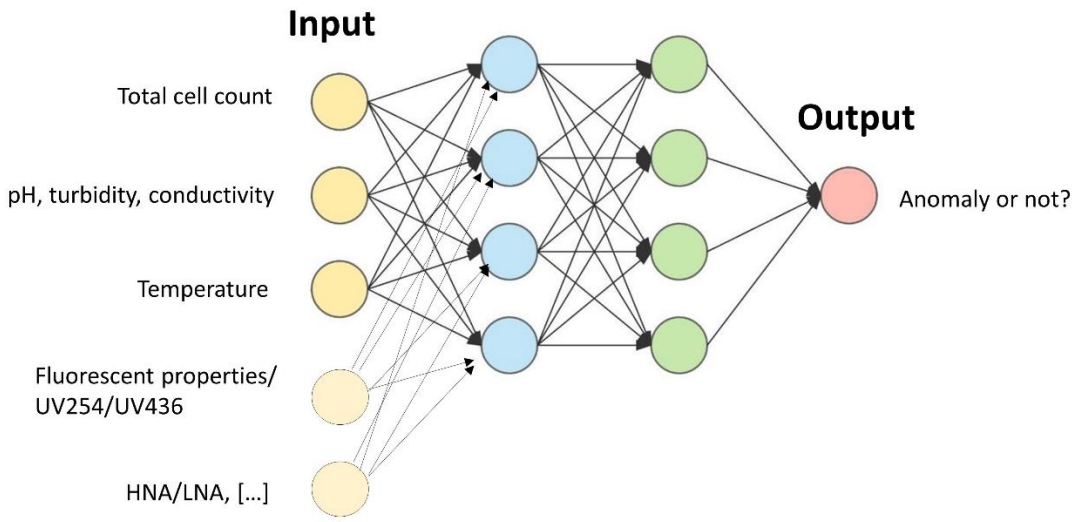

Figure 9: Conceptual layout of ANN where input features are water quality parameters that can be measured online and the output is a prediction of a possible anomaly in the water network system.

After the first pre-processing and evaluation of the water quality data, the correlation of various parameters was conducted to understand for which parameter it is reasonable to train the ANN. Although a significant amount of data was provided, there was still a lack of various organic water quality parameters in the dataset. The sparse dataset was imputed with the k-Nearest Neighbor Imputation method. After preparing the data, an ANN and random forest algorithm were trained to predict water quality anomalies. The accuracy of the random forest algorithm for predicting a water event came out to 97% which is considerably very high. However, it must be acknowledged that it came from primarily true negatives, not true positive water event predictions.

Utilizing a data-driven model as a support tool for water utilities is a promising technology. It should be explored further with support from Hamburg Wasser, who can evaluate the use they could have from it as a water utility. However, due to insufficient data, WP-3 was not explored further for contamination detection in WDS in this project.

WP4: Modeling framework for sensor placement and source detection.

Computer-based physical modeling tools that simulate water quality variations in WDS are functional solutions for monitoring WDS integrity and adequately fit the framework for sensor placement locations identification and detecting contamination events. WP-4 developed EPyT-C (in which C stands for any contaminant), a Python-based package allowing the simulation of the transport and fate of multiple water quality parameters in WDS. EPyT-C constitute in-built modules that conceptualize the scientific understanding of the physical, physicochemical, and biochemical interactions concerning water quality parameters within the distribution network realm, mathematize them as one-dimensional advective-reactive equations, and numerically solve them to emulate the spatiotemporal distribution of the quality of water delivered via WDS.

EPyT is an open-source software, initially developed by the KIOS Research and Innovation Center of Excellence, University of Cyprus, operating within the Python environment to

provide a programming interface for the latest version of EPANET 2.2 (Rossman et al., 2020). It calls EPANET a shared object and employs an Object-Oriented approach for interfacing EPANET with Python. Though EPyT can be employed for performing single-species water quality analysis, which comes within the scope of EPANET 2.2, it lacks MSRT modeling capability in its current form. In other words, EPyT can only analyze one water quality parameter at a time. Consequently, the water quality modeling compartment of EPyT needs to be improved to solve several real-world problems concerning water quality variations during delivery via WDS. A fully independent water quality modeling extension, EPyT-C, is developed in this direction. The source code of EPyT-C calls EPyT and employs the hydraulic solver of EPANET 2.2 for performing hydraulic simulation, which the in-built water quality solver then utilizes for performing MSRT modeling.

In its current form, EPyT-C comprises two in-built modules - the 'Chlorine decay and Trihalomethanes formation' module and the 'Bacterial regrowth' module. The former EPyT-C module encompasses all the required details on the physical and physicochemical interactions of the following three water quality parameters: free available chlorine (FAC), total organic carbon (TOC), and trihalomethanes. The latter contains details on the physical, physicochemical, and biochemical interactions of the five water quality parameters: FAC, recalcitrant dissolved organic carbon, biodegradable dissolved organic carbon, free-living bacteria (suspended heterotrophic bacteria), and free dead bacteria. Based on the module selected for WDS analysis, EPyT-C evolves partial differential equations and ordinary differential equations governing the propagation and formation/ degradation of the corresponding water quality parameters within the distribution network realm. Once the governing equations (advective-reactive equations) are framed, the numerical method that involves the explicit method of characteristics and the fourth-order Runge-Kutta method is applied to derive numerical solutions – spatiotemporal distribution of complex water quality parameters in WDS.

EPyT-C offers the following flexibilities, making it a handy tool for research and industry: 1. Allows time-series variations in the input values for the water quality parameters at the sources (reservoirs and booster nodes). 2. Customize the random fluctuations in the input values for the water quality parameters at the sources. 3. Customize the perturbations in the reaction rate coefficient values. 4. Customize the outputs and export the data as Excel files or other formats (Figure 10). 5. Customize the numerical accuracy by altering the model parameters (time step, velocity tolerance, etc.). 6. Control the computational efficiency by adjusting the accuracy of the numerical solutions.

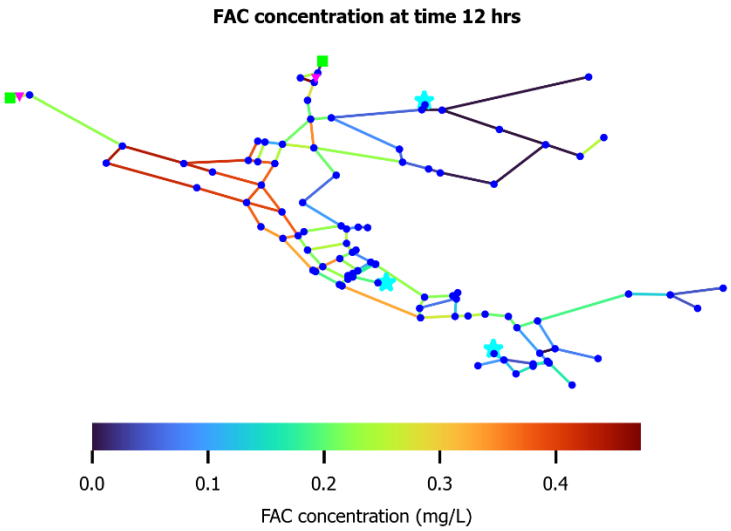

Figure 10: Spatial distribution of FAC at time = 12 hours within the benchmark test network (EPANET Network 3) corresponding to FAC concentration 0.5 mg/L at the river and lake water source outlets. The TOC concentration values at the river and lake sources outlets were maintained at 3 mg/L and 1 mg/L, respectively. The simulations were performed using the 'Chlorine decay and Trihalomethanes formation' module of EPyT-C. The squares denote reservoirs, stars indicate tanks, and circles indicate junctions. The lines specify links connecting reservoirs, tanks, and nodes.

In conclusion, EPyT-C is a practical tool that can assist the scientific community and water utility managers in examining WDS performance under different operating scenarios. EPyT-C scripts are under continuous development and can be further extended and improved by users and developers for specific applications. Forthcoming works involve advancing EPyT-C modeling capability to simulate dispersive transport.

TUIL

Hao Cao, and Pu Li

WP1: Modeling of the water quality

In the first working package, a water quality model has been developed for the optimization model in the following. For the water quality of WDS, a one-dimensional advection equation with reaction is very common to be used:

$$\frac{\partial C_i(x,t)}{\partial t} u_i \frac{\partial C_i(x,t)}{\partial x} + rC_i(x,t) = 0 \tag{4}$$

where $C_i(x,t)$ = chlorine concentration inside the pipe i at point x and time t ; u_i = flow velocity in the pipe i with changing sign as the flow changes its direction, r = reaction coefficient which is pipe-dependent for a component such as chlorine for example, which is named as bulk and wall reaction (Rossman et al. 1994). Since

$$\frac{\partial C_i}{\partial t} = \frac{\partial C_i}{\partial x}\frac{\partial x}{\partial t} + \frac{\partial C_i}{\partial t}$$

$$= u\frac{\partial C_i}{\partial x} + \frac{\partial C_i}{\partial t} = rC_i \tag{5}$$

$$C_i(x(t), t) = C_{i0}e^{rt}$$

Function (5) reveals that the chlorine concentration change in a WDS is a decay process, i.e. the concentration at a position within a pipe can be calculated by the time it takes for the water to travel from the starting of the pipe to this position. With the help of this function, the component (chlorine) concentration at every node depends on the initial value, reaction coefficient *r* and time *t*.

In the work that followed, Function (5) is used as a simplified water quality model in optimization models.

WP2: Nonlinear optimization model

In this working package, a nonlinear optimization problem was formulated based on hydraulic and water quality, numerically implemented, and solved to achieve the specified chlorine concentration within a reasonable range in a WDS.

Hydraulic characteristics include several parameters of the WDS, such as pressure, head loss and flow. One of the most important parameters for water quality control is the flow velocity in the pipes. EPANET can be used for calculating the velocity, but it is challenging to use its results for solving optimization problems. Two new methods were proposed to obtain a suitable form that can be applied to the water quality model and optimization. The Hardy cross method (Brkić et al. 2019) is a classic iterative method for determining the flow in pipe networks. We proposed the maximization of energy conservation as a novel method to compute the flow in a pipe network. In addition, the flow control valve (FCV) is one of the most critical actuators of the WDS with the control system. Therefore, we proposed to manipulate and redistribute the flow velocity in the pipelines with the FCV.

For this purpose, a nonlinear optimization problem was formulated based on the hydraulics and water quality model, numerically implemented, and solved to achieve the specified chlorine concentration within a reasonable range in a WDS. The mass and energy conservation laws were employed to describe the hydraulic properties of WDSs. The one-dimensional advection transport model was simplified to describe the decay of chlorine in the pipelines. The chlorine concentration limits at the nodes were formulated as inequality constraints which will be satisfied by manipulating the flows and their directions in the pipelines. The optimization problem is expressed as follows:

$$\begin{aligned} &\min_{q_1 \ldots q_{np}} \frac{1}{2}\sum_{c=1}^{n_c}\left(\sum_{j=1}^{n_p} L_{cj}k_j\left|q_j\right|^{1.852}\right)^2 \\ &subject\ to: NQ = D \\ &Lower\ limit < Ci < Upper\ limit \\ &0 \le \left|q_j\right| \le q_{max}, \forall j = 1, \ldots, n_p \end{aligned} \tag{6}$$

where $|q|_j$ is the flow rate in pipe *j.* The absolute value here is to consider changes in the flow direction. The equality constraint and the inequality constraint are used to describe the constraint of flow rate in each pipe and chlorine concentration at certain nodes. A model-based optimal control strategy was developed based on this optimization model. The interior point solver (IPOPT) for large-scale nonlinear optimization (Waechter et al. 2006) was used to solve the nonlinear optimization problem. Figure 11 shows a selected benchmark network model 1 with two loops, A-B-F-E and A-C-D-B as a case study.

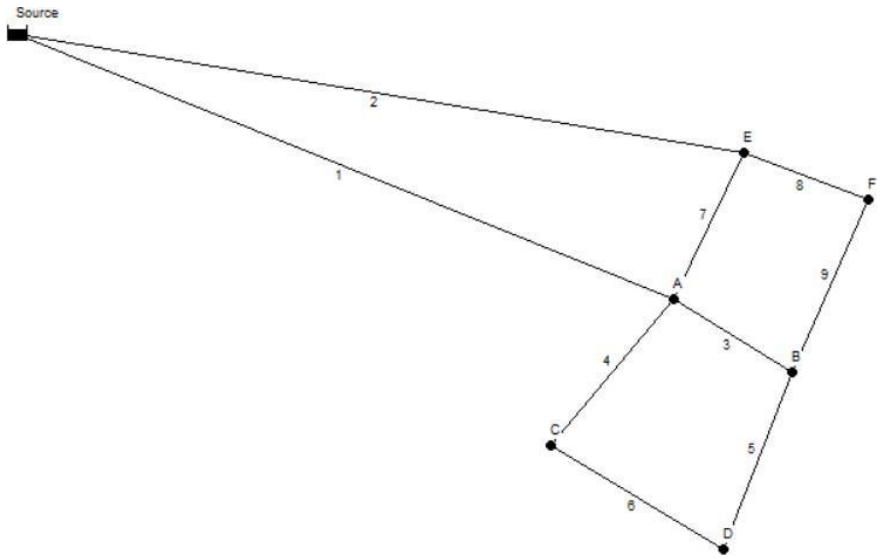

Figure 11: WDS with two loops.

The whole system has one reservoir, 6 nodes, and 9 pipes. Assuming a chlorine concentration of 1.2 mg/L in the reservoir and node concentrations should be between 0.1 - 0.3 mg/L. In the operation, the concentrations at some nodes are outside this range and we aim to compute a new operation strategy so that they go back to the specified range. The elevation of the reservoir and all other nodes are 80 m and 5 m, respectively. All pipes have the same diameter and roughness of 500 mm and 100. The length of pipes 1 and 2 is 13,608 m and all other pipes are 2,268 m.

Table 2: Results of model 1.

Node ID	Demand $(\mathbf{m^3/h})$	Chlorine concentration (mg/L)		Pipe ID	Flow rate $(\mathbf{m^3/h})$	
		Original system	After FCV Placement		Original system	After FCV Placement
Reservoir		1.2	1.2	1	100.2	114.5

A	0	0.35	0.45	2	99.82	86.10
B	30	0.21	0.24	3	54.23	54.55
C	30	0.26	0.30	4	63.53	44.81
D	80	0.14	0.16	5	46.46	65.38
E	30	0.39	0.30	6	33.53	14.71
F	30	0.27	0.23	7	17.59	-15.02
				8	52.22	71.03
				9	22.23	40.93

Table 2 shows the results of solving the optimization problem. In the original operation, at node E, the concentration is higher than 0.3 mg/L. Using the optimized operation with the FCVs placement, each node now has an acceptable chlorine concentration. In comparison to the original operation, there is a significant change in the flow rate in each pipe, even with a change in flow direction in pipe 7. This means that chlorine concentration has been effectively controlled by the FCVs placement.

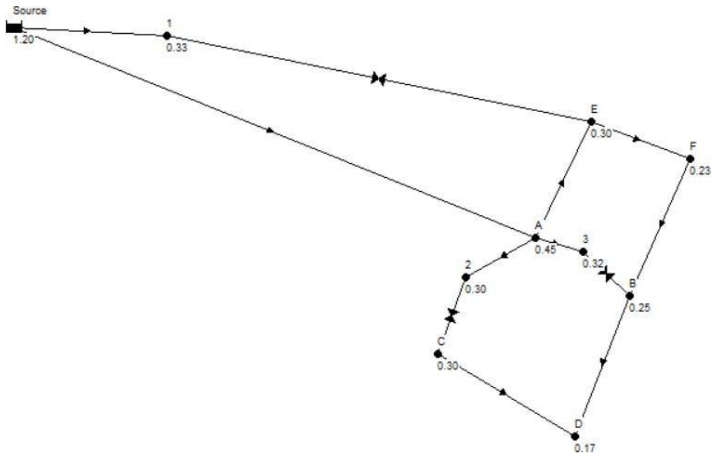

Figure 12: WDS with two loops with FCV placement.

Figure 12 shows the FCV arrangement and the simulation result from EPANET, with three FCVs installed in the WDS, and the chlorine concentration of each node. Compared to the calculation results in Table 3, the error of concentration of chlorine at each node from the simulation is very small. The results of this section give us a way to use FCV in water quality control and thus water quality management by controlling the flow rate as well as the direction in the pipes.

WP3: MINLP Optimization model

A MINLP approach was developed in this working package to optimize the placement of isolation valves. We aim to keep the chlorine concentration in the specified range in the

network. The simplified one-dimensional advective transport model describes the decay of chlorine in the pipes, and the mass and energy conservation laws are enforced as nonlinear constraints. In addition, binary variables are used to describe the placement of valves as possible isolation valves that can either be opened or closed. The MINLP problem is defined as follows:

$$\min \ Amount(i) \tag{7a}$$

$$\text{subject to: } Nq - D = 0, \tag{7b}$$

$$q(-N^T P - N^T e - h_f(q)) \geq 0, \tag{7c}$$

$$-N^T P - N^T e - h_f(q) - Mz \leq 0, \tag{7d}$$

$$z_j + z_{n_p+j} \leq 0, \qquad \forall j = 1,\ldots,n_p, \tag{7e}$$

$$\sum_{j=1}^{2n_p} z_j = n_v, \tag{7f}$$

$$\sum_{j=1}^{2n_p} q_j z_j = 0, \qquad \forall j = 1,\ldots,n_p, \tag{7g}$$

$$P_{\min} \leq P_i \leq P_{\max}, \qquad \forall i = 1,\ldots,n_n, \tag{7h}$$

$$0 \leq q_j \leq q_{\max}, \qquad \forall j = 1,\ldots,n_p, \tag{7i}$$

$$Concentration_{\min} \leq Concentration_i \leq Concentration_{\max}, \quad \forall i = 1,\ldots,n_n, \tag{7j}$$

$$z \in \{0,1\}^{2n_p}, \tag{7k}$$

where the objective function (7a) is to minimize the chlorine amount to be injected into the WDS at position *i*. n_n and n_p are number of nodes and pipes in the WDS. To ensure the hydraulic feasibility of the solution, (7b) expresses the mess conservation law of each node, (7c) and (7d) consider the energy conservation law of each pipe with and without isolation valve, respectively. The flow direction can be changed due to the valve arrangement, therefore the node-pipe incidence matrix is N ∈ R2np×nn. $h_f(q)$ is the head loss of each pipe, for which the Hazen–Williams equation is used in this study. q_j and P_i are flow and pressure on every pipe or node. z_j is a {0, 1} vector, that expresses there is no isolation valve or there is one. Each segment is a constant to express the head loss on isolation valves, since the valves are closed after placement, M in (7d) is a large enough value in this study. The inequality (7e) is a constraint to guarantee that only one valve is allowed to be placed on each pipe, and the quality constraint (7f) considers the total number of valves to be placed in the network n_v. The equality (7g) describes the pipe with an isolation valve having no more flow. The minimum and maximum pressure and flow in each node and pipe are defined by (7h) and (7i), respectively. (7j) is the constraint of chlorine concentration at a certain node. (7k) is the binary constraint to specify whether or not a valve is fitted on a pipe. In this study, Bonmin has been used to solve the MINLP model (Bonami et al. 2011.)

The MINLP model is implemented and validated by using a benchmark WDS shown in Figure . The lower bound of residual chlorine concentration and pressure was set to 0.45mg/L, and

20m, respectively. The optimization result is shown in Table 3 and Table 4. In the first step, no valve is considered in the WDS as the initial scenario, i.e., in the MINLP model$n_v = 0$. It can be seen from Table that the minimum chlorine concentration is maintained, but the sum of residual chlorine in the WDS is quite high. Generally speaking, the more valves installed in the WDS, the less the total amount of chlorine that needs to be injected into the water source to maintain the minimum concentration of WDS residual chlorine, and the lower the maximum concentration, as well as the total sum of residual chlorine in the system. However, the difference between the results of using 1 to 3 valves and 4, to 5 valves is not significant, as shown in Table 3. The reason may be due to the fact that the MINLP model is not convex and thus the solver cannot guarantee a global solution.

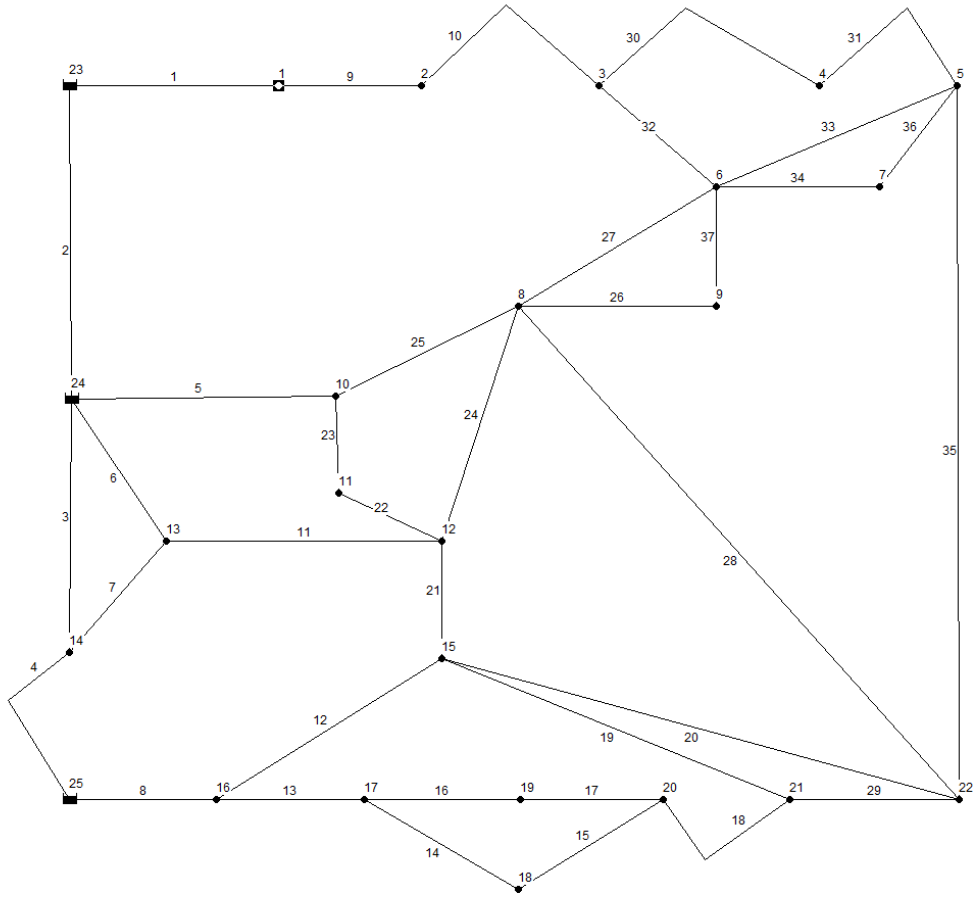

Figure 13: A benchmark water network.

Table 3: Number of valves to be used and the corresponding chlorine concentration.

Concentration (mg/L)	0 valve (Initial)	1 valve	2 valves	3 valves	4 valves	5 valves
Reservoirs (23,24,25)	1.35	0.96	0.96	0.96	0.7	0.7
Minimum in WDS	0.45	0.45	0.45	0.45	0.45	0.45

Maximum in WDS	1.30	0.93	0.93	0.93	0.68	0.68
Sum of residual Chlorine	22.42	16.19	16.19	16.5	12.56	12.63

Table 4: Number of valves and their position.

Number of valve(s)	Position of the valve (Pipe ID)
1	31
2	31,35
3	12,31,35
4	10,20,31,35
5	10,19,20,31,35

Table 4 shows the resulting optimal positions of the valves. It can be seen that there are several pipes, such as 31, and 35, have always been chosen, which means that such pipelines have a higher potential to affect the residual chlorine.

The results of this section lead to a method to place isolation valves in water quality control so that the concentration of disinfectant in the water can be controlled by closing or opening specific pipes, thus affecting the quality of the water. This method can also be used to design control strategies after contamination in the WDS to separate the contaminants and reduce their impact.

WP4: Testbed design and construction

A testbed to verify the computed control strategy was designed and constructed. Figure 14 shows the structure of the testbed.

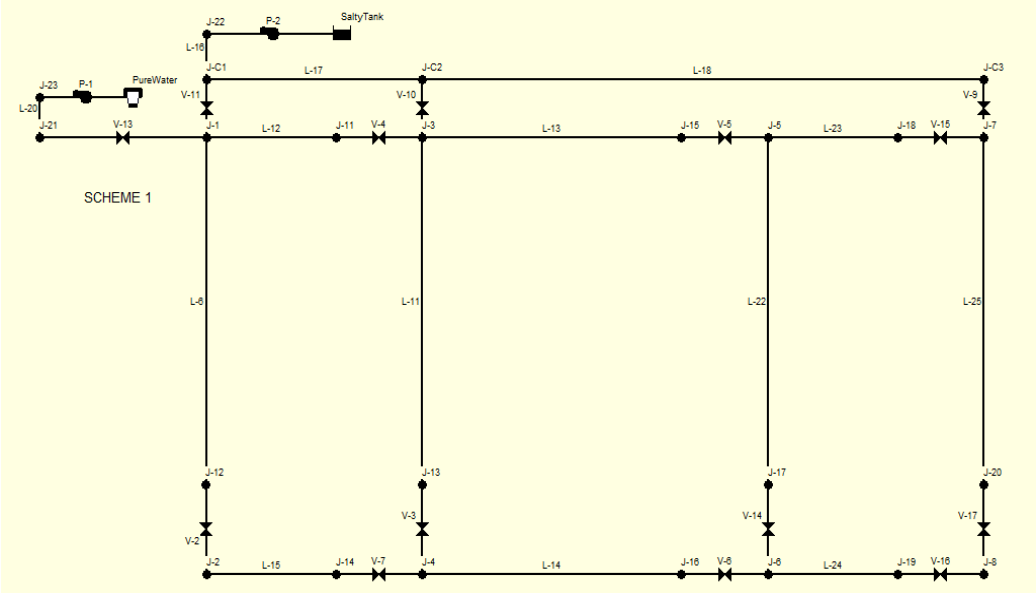

Figure 14: Structure of the testbed.

The entire network includes water tanks, pumps, valves, pressure sensors, water quality sensors, and flow sensors. For the first study, we plan to study the case of bringing salty water into the system as a contaminant and detected by the conductivity sensors in the system. Then the valves and pumps are manipulated by the control strategy to reduce the contamination in the possibly shortest time.

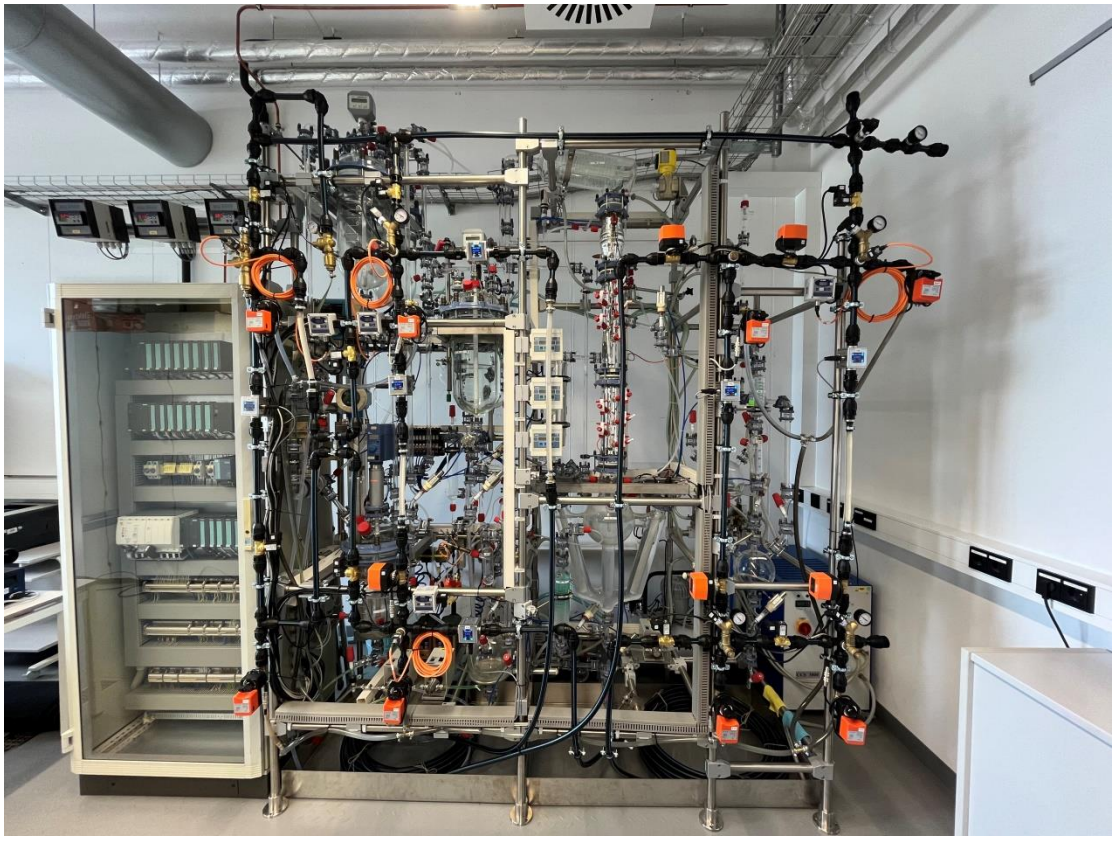

Figure 15: TU Ilmenau testbed.

Figure 15 shows the constructed testbed. Figure 16 is the monitoring software interface of the testbed established.

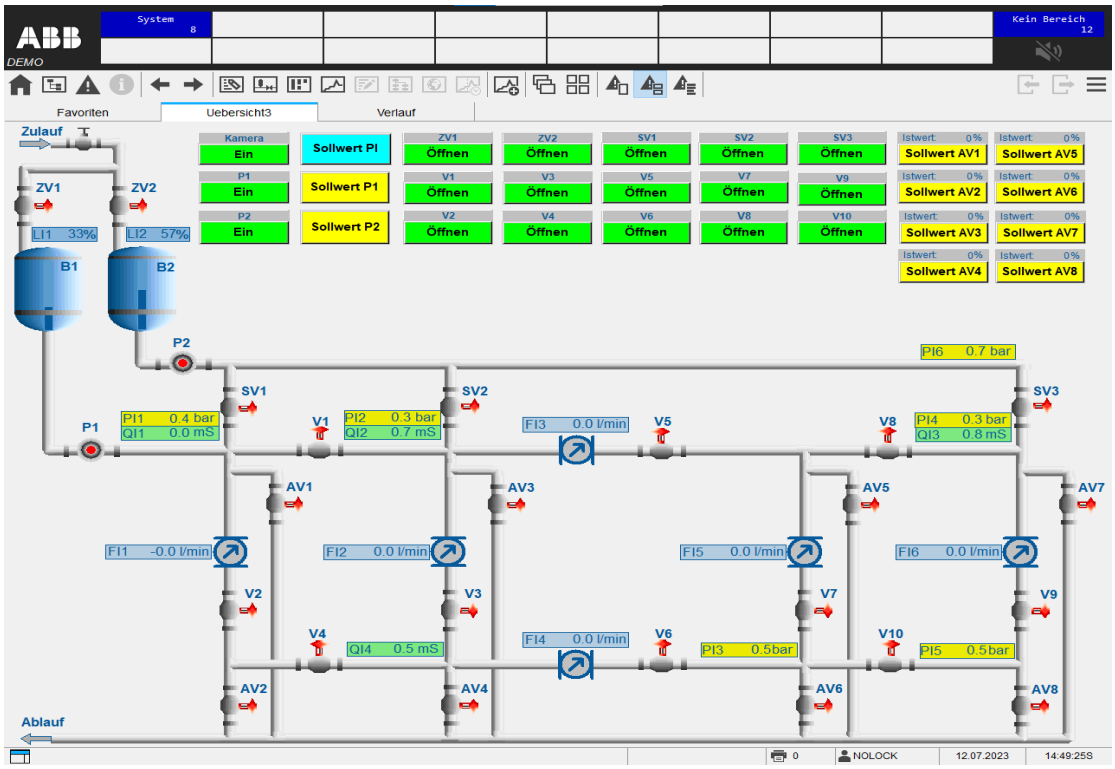

Figure 16: Monitoring interface of the testbed.

WP5: Experiment on testbed

After the testbed construction was completed, experiments were conducted to test the pipe flushing in case of contamination. In addition, we designed a control system to realize the manipulation of this testbed.

Many different scenarios of contamination were tested. Fig. 17 shows the experimental results of one scenario of contamination. It includes 8 time-dependent trajectories, which are the water quality, water pressure, and control signal of the valves and pumps, respectively. At the bottom of the last graphic, the time points of T1 to T5 are marked. In this scenario, we assume that the contamination happened from T1 to T2, then an alarm was given at that moment. From T3 to T5 different actions of the valves separated (isolated) the contamination and then flushed the pipes. It is seen from the first graphic that, from T5, the water quality was within the specified range, i.e., the WDS was recovered to normal operation.

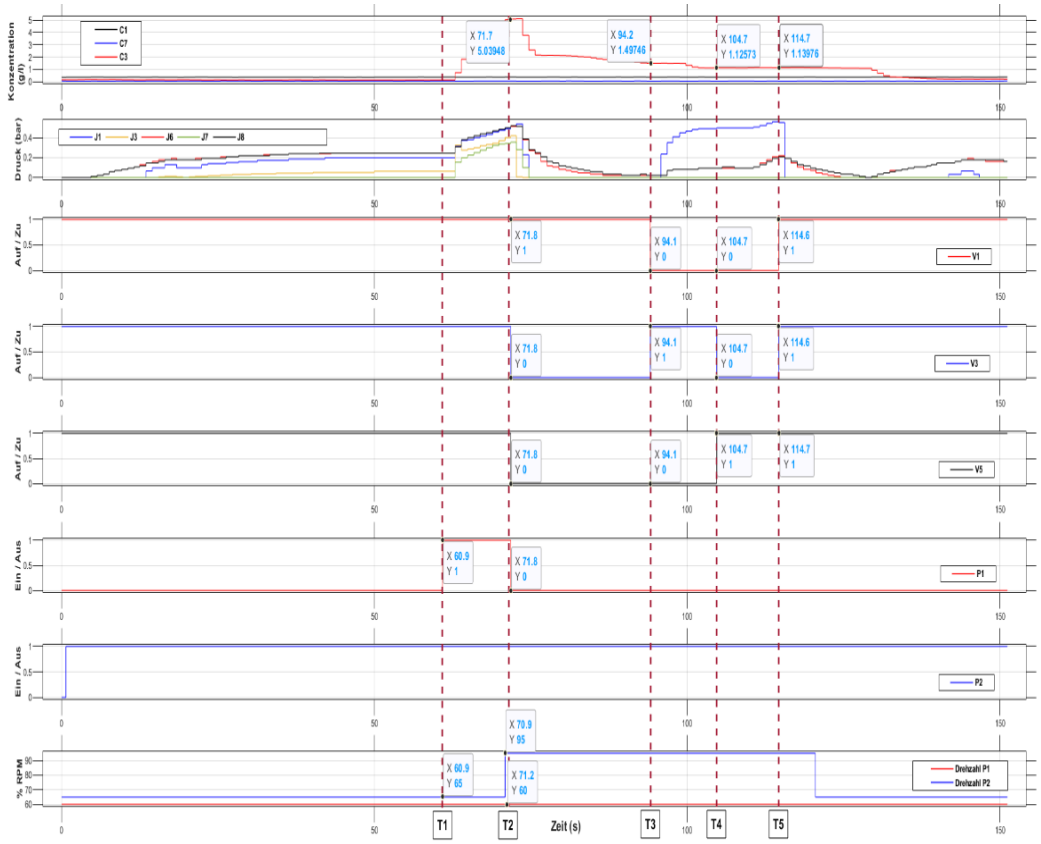

Figure 17: Signals of pollution and flushing process of the testbed.

Joint conclusions

The MoDiCon project aimed the development of a future digitalized WDS and its main challenges of dealing with crucial water quality change. With respect to the rapid characterization of the water quality, the combination of flow cytometry and fluorescence spectroscopy (including PARAFAC) was proven as a successful method that can be implemented in future standardized applications. The further development showed the opportunities for detailed organic and microbial fingerprinting. Even little changes in water matrices are possible to detect, thus, contaminated water can be further characterized. The computer-based tools capable of simulating the quality fluctuations that can act like digital twins are critical for developing digitized WDS. The real-world data paucity is a limiting factor in developing data-driven modeling tools in this regard. Conversely, the development and performance of physics-based models were found to be significantly impacted by numerous factors such as water temperature, type of microbial species present, growth-limiting nutrients availability, the presence of residual disinfectant and other inhibitory substances; microbial attachment/ detachment to/from the pipe walls; biofilm formation; particle deposition; and sediment re-suspension. Within these limitations, the physics-based models developed could adequately forecast microbiological water quality in WDS, specifically total cell count (TCC). Due to the many processes considered and the interrelation between the model parameters signifying the mechanisms governing water quality, the reliability of predictions of the physics-based models was found to be highly sensitive to epistemic uncertainty. Forthcoming works involve advancing modeling capability

to simulate and predict different water quality parameters within the WDS. These computer-based simulation tools, combined with installed flow cytometry and fluorescence spectroscopy, enable the monitoring and prediction of water quality all over the network. Actual measuring, as well as simulating of water quality, were interfaced with reaction and controlling methods. Therefore, individual characteristic baseline limits were established for flow cytometric and fluorescence spectrometric (PARAFAC) parameters. Considering autonomous controlling, two new optimization methods were proposed. For both, successful simulations were performed and showed the potential of those implanting in a real WDS. Furthermore, a newly designed test bed was used to simulate different automated contamination and reaction processes in a small-scale network.

In terms of applying the MoDiCon outcomes to the real world, it has to be mentioned, that the developed systems need to be further tested under real circumstances such as in a real WDS. Although the individual methods are sufficiently developed and evaluated in a common laboratory and pilot plant framework, especially the communication between measured values, simulation, and reaction must be validated for a real WDS. Furthermore, bringing the developed methods into practice faces several application challenges. In particular, the conversion of automated monitoring stations, valves, and control equipment required a great deal of work as well as expenses. In addition, employees of water utilities must also have the appropriate qualifications to be able to work with such automated systems. However, other research groups and water suppliers can use published methodologies based on the MoDiCon outcome to improve water quality surveillance.

2. PUBLICATIONS, PATENTS, INVENTIONS:

Journal publications:

Abhijith, G. R., and Ostfeld, A. 2023. Assessing uncertainties in mechanistic modeling of quality fluctuations in drinking water distribution systems. ASCE Journal of Environmental Engineering (Accepted for publication).

Ostfeld, A., and Abhijith, G. R. 2023. Digital Twin for Water Distribution Systems Management—Towards a Paradigm Shift. ASCE Journal of Pipeline Systems Engineering and Practice Forum, 14(3), 02523001. https://doi.org/10.1061/JPSEA2.PSENG-1486 Date of publication: May 13, 2023.

Abhijith GR, Salomons E, Ostfeld A. 2022. Reliability of a Contamination-Detection Sensor Network in Water Distribution Systems during a Cyber-Physical Attack. Water. 2022; 14(22):3669. https://doi.org/10.3390/w14223669. Date of publication: November 14, 2022.

Abhijith, G. R., and Ostfeld, A. 2022. Flexible decision-making framework for developing operation protocol for water distribution systems. Journal of Environmental Management, 320, 115817. https://doi.org/10.1016/j.jenvman.2022.115817. Date of publication: October 15, 2022.

Abhijith GR, Ostfeld A. 2022. Contaminant Fate and Transport Modeling in Distribution Systems: EPANET-C. Water. 2022; 14(10):1665. https://doi.org/10.3390/w14101665. Date of publication: May 23, 2022.

Abhijith, G. R., and Ostfeld, A. 2022. Making Waves: Applying Systems Biology Principles in Water Distribution Systems Engineering. Water Research, 219, 118527. https://doi.org/10.3390/w13040463. Date of publication: July 1, 2022.

Abhijith, G.R.; Kadinski, L.; Ostfeld, A. Modeling Bacterial Regrowth and Trihalomethane Formation in Water Distribution Systems. Water 2021, 13, 463. https://doi.org/10.3390/w13040463. Date of publication : February 10, 2021.

Abhijith, G.R., Ostfeld, A. 2022. Examining the Longitudinal Dispersion of Solutes Inside Water Distribution Systems. J. Water Resour. Plan. Manag. 148, 04022022. https://doi.org/10.1061/(ASCE)WR.1943-5452.0001562. Date of publication: March 21, 2022.

Abhijith, G.R.; Ostfeld, A. Modeling the Formation and Propagation of 2,4,6-trichloroanisole, a Dominant Taste and Odor Compound, in Water Distribution Systems. Water 2021, 13, 638. https://doi.org/10.3390/w13050638. Date of publication: February 27, 2021.

Abhijith, G.R., Ostfeld, A. 2021b. Modeling the Response of non-chlorinated, Chlorinated, and Chloraminated Water Distribution Systems toward Arsenic Contamination. J. Environ. Eng. 147, 04021045. https://doi.org/10.1061/(asce)ee.1943-7870.0001918. Date of publication: August 12, 2021.

Abhijith, G.R., Ostfeld, A. 2021c. Model-based investigation of the formation, transmission, and health risk of perfluorooctanoic acid, a member of PFASs group, in drinking water distribution systems. Water Res. 204, 117626. https://doi.org/10.1016/j.watres.2021.117626. Date of publication: October 1, 2021.

Schuster, J., Huber, J., Stumme, J., Grieb, A., & Ernst, M. 2022. Combining real-time fluorescence spectroscopy and flow cytometry to reveal new insights in DOC and cell characterization of drinking water. Frontiers in Environmental Chemistry, 3. https://doi.org/10.3389/fenvc.2022.931067. Date of publication: August 30, 2022.

Conference proceedings:

“Optimal placement of isolation valves in water distribution system to ensure water quality”, Cao, H., Li, P., 19th International Computing & Control for the Water Industry Conference, Leicester, UK., September 4-7, 2023.

“Hybrid mechanistic and machine learning-based modeling approach for predicting quality fluctuations in drinking water distribution systems”, Abhijith, G. R., Ivo, D., Cominola, A., and Ostfeld, A., 19th International Computing & Control for the Water Industry Conference, Leicester, UK., September 4-7, 2023.

“Introducing EPyT-C: An independent Python-based water quality modeling extension for EPANET” Abhijith, G. R. and Ostfeld, A. 19th International Computing & Control for the Water Industry Conference, Leicester, UK., September 4-7, 2023.

“Exploring the cause-effects of quality fluctuations in drinking water distribution systems by applying systems biology approaches”, Abhijith, G. R., Leonidou, N., Dräger, A., and Ostfeld, A., 19th International Computing & Control for the Water Industry Conference, Leicester, UK., September 4-7, 2023.

“Design and test of an experimental facility for water quality control in water supply network”, Cao, H., Saticiöz, T., Hollandmoritz, J., and Li, P., African International Conference on Machine Learning, Optimization and Applications, Kigali, Ruwanda, Agust, 2023

“Inferring the stochasticity associated with modeling the biological stability of drinking water within distribution networks”, Abhijith, G. R. and Ostfeld, A. World Environmental and Water Resources Congress 2023: Adaptive Planning and Design in an Age of Risk and Uncertainty, Henderson Nevada, USA., May 21-24, 2023.

“Enhancing the reliability of a contamination detection sensors network in water distribution systems during a cyber-attack”, Abhijith, G. R., Salomons, E., and Ostfeld, A. World Environmental and Water Resources Congress 2023: Adaptive Planning and Design in an Age of Risk and Uncertainty, Henderson Nevada, USA., May 21-24, 2023

„Towards digital twins for emerging contaminants in water distribution systems”, Abhijith, G. R., Steffelbauer, D., and Ostfeld, A. World Environmental and Water Resources Congress 2023: Adaptive Planning and Design in an Age of Risk and Uncertainty, Henderson Nevada, USA., May 21-24, 2023.

“A machine learning-based surrogate model for coupled hydraulic and water quality simulation in water distribution networks”, Ivo, D., Kadinski, L., Abhijith, G. R., Ostfeld, A., and Cominola, A. World Environmental and Water Resources Congress 2023: Adaptive Planning and Design in an Age of Risk and Uncertainty, Henderson Nevada, USA., May 21-24, 2023.

„Online monitoring and digital control in drinking water distribution systems“, Schuster, J., Kadinski, L., Cao, H., Abhijith, G. R., Li, P., Ostfeld, A., & Ernst, M. (2022). MOST-BMBF Cooperation in Water Technology Research, 35–41. https://www.fona.de/medien/pdf/Proceedings-StatusSeminar2022-24-10-2022-web.pdf?m=1666591523&

“Machine Learning Methodologies to Predict Possible Water Quality Anomalies as a Support Tool for Online Monitoring of Organic Parameters”, Kadinski L., Schuster J., Abhijith G. R., Cao H., Grieb A., Meier T., Pu L., Ernst M., Ostfeld A., International Joint Conference on Water Distribution, Valencia, Spain, 2022.

“Appraisal of the Position of Water Distribution Systems as a PFAS Exposure Pathway”, Abhijith, G. R. and Ostfeld, A. World Environmental and Water Resources Congress 2022, Atlanta, GA, USA, June 5-8, 2022.

“EPANET-C—An Umbrella Simulation Tool for Water Distribution System Quality Analysis”, Abhijith, G. R. and Ostfeld, A. World Environmental and Water Resources Congress 2022, Atlanta, GA, USA, June 5-8, 2022.

“Establishing an experimental and simulation interface for online monitoring and modelling of bacterial growth in water distribution systems”, Kadinski L., Schuster J., Abhijith G. R., Cao H., Grieb A., Pu L., Ernst M., Ostfeld A., World Environmental and Water Resources Congress 2022, Atlanta, GA, USA, June 5-8, 2022.

“Real-time monitoring and controlling of water quality in water distribution networks based on flow cytometry and fluorescence spectroscopy”, Schuster J., Kadinski L., Cao H., Abhijith G. R., Grieb A., Pu L., Ostfeld A., Ernst M., World Environmental and Water Resources Congress 2022, Atlanta, GA, USA, June 5-8, 2022.

“Optimal control of chlorine concentration in water distribution systems”, Cao H., Schuster J., Kadinski L., Abhijith G. R., Grieb A., Ernst M., Ostfeld A., Pu L., World Environmental and Water Resources Congress 2022, Atlanta, GA, USA, June 5-8, 2022.

“Real-time Trinkwasseranalyse mittels Durchflusszytometrie und Fluoreszenzspektroskopie“, Schuster J., Backes H., Grieb A., Ernst M., Wasser 2022 – Jahrestagung der Wasserchemischen Gesellschaft, 223-229. https://www.wasserchemische-gesellschaft.de/de/wasser-2022/seiten/wasser-2022.

3. REFERENCES

Asheri Arnon, T., Ezra, S., and Fishbain, B. (2019). “Water characterization and early contamination detection in highly varying stochastic background water, based on Machine Learning methodology for processing real-time UV-Spectrophotometry.” .Water Research, Elsevier Ltd, 155, 333–342

Ashwini, C., Singh, U. P., Pawar, E., and Shristi. (2019). “Water quality monitoring using machine learning and IoT.” International Journal of Scientific and Technology Research, 8(10), 1046–1048.

Bonami, Pierre & Lee, Jon. (2011). BONMIN Users' Manual.

Brkić, D.; Praks, P. Short Overview of Early Developments of the Hardy Cross Type Methods for Computation of Flow Distribution in Pipe Networks. Appl. Sci. 2019, 9, 2019. https://doi.org/10.3390/app9102019

Efstratiou, A., Ongerth, J. E., & Karanis, P. (2017). Waterborne transmission of protozoan parasites: Review of worldwide outbreaks - An update 2011–2016. *Water Research*, *114*, 14–22. https://doi.org/10.1016/j.watres.2017.01.036

Eliades, D. G., Kyriakou, M., Vrachimis, S., and Polycarpou, M. M. (2016). "EPANET-MATLAB Toolkit : An Open-Source Software for Interfacing EPANET with MATLAB." 1–8.

Hammes, F. A., and Egli, T. (2005). “New method for assimilable organic carbon determination using flow-cytometric enumeration and a natural microbial consortium as inoculum.” Environmental Science and Technology, 39(9), 3289–3294.

Moreira, N. A., & Bondelind, M. (2017). Safe drinking water and waterborne outbreaks. *Journal of Water and Health*, *15*(1), 83–96. Scopus. https://doi.org/10.2166/wh.2016.103

Murphy, K. R., Stedmon, C. A., Graeber, D., & Bro, R. (2013). Fluorescence spectroscopy and multi-way techniques. PARAFAC. *Analytical Methods*, *5*(23), 6557–6566. https://doi.org/10.1039/c3ay41160e

Prest Emmanuelle I., Hammes Frederik, van Loosdrecht Mark C. M., Vrouwenvelder Johannes S.(2016) Biological Stability of Drinking Water: Controlling Factors, Methods, and Challenges. Frontiers in Microbiology. 7,45. doi: 10.3389/fmicb.2016.00045

Rossman, Lewis et al. Epanet users manual. 1994.

Rossman, L. A., H. Woo, M. Tryby, F. Shang, R. Janke, and T. Haxton. 2020. EPANET 2.2 user’s manual. Cincinnati: USEPA.

Schuster, J., Huber, J., Stumme, J., Grieb, A., & Ernst, M. (2022). Combining real-time fluorescence spectroscopy and flow cytometry to reveal new insights in DOC and cell characterization of drinking water. *Frontiers in Environmental Chemistry*, *3*. https://doi.org/10.3389/fenvc.2022.931067

Waechter, Andreas & Biegler, Lorenz. On the implementation of an interior-point filter line-search algorithm for large-scale nonlinear programming. Mathematical programming, 106:25–57, 03 2006.

White, S., Quinn, J., Enzor, J., Staats, J., Mosier, S. M., Almarode, J., Denny, T. N., Weinhold, K. J., Ferrari, G., & Chan, C. (2021). FlowKit: A Python Toolkit for Integrated Manual and Automated Cytometry Analysis Workflows. *Frontiers in Immunology*, *12*, 4652–4652. https://doi.org/10.3389/FIMMU.2021.768541/BIBTEX

Zhang W, Miller CT, Digiano FA, Asce M (2004) Bacterial Regrowth Model for Water Distribution Systems Incorporating Alternating Split-Operator Solution Technique. J Environ Eng 130:932–941

WT1902
NanoElectroMembrane processes for micropollutant removal in WAter REuse

COVER SHEET (SIGNED BY THE PRINCIPAL INVESTIGATORS)

Federal Ministry of Education and Research (BMBF), Germany	**Ministry of Science, Technology and Space (MOST), Israel**

Joint German-Israeli Water Technology Research Program

JOINT FINAL REPORT

For the Period: June 2020 until Dec 2023 (Final report)

German Project Number FE.5276.0001.343 Israeli Project Number 3-17010

Title of German Project: Nano-electro membrane processes for micropollutant removal in water reuse

Title of Israeli Project: Nano-electro membrane processes for micropollutant removal in water reuse

Principal Investigator(s) -- including Institution(s) and Department(s):

Prof. Daniel Mandler
The Hebrew University of Jerusalem (HUJI), Institute of Chemistry

Prof Dr. Ing Andrea Iris Schäfer
Karlsruhe Institute of Technology (KIT), Institute for Advanced Membrane Technology (IAMT)

Signatures:
Israeli Principal Investigator(s):

Daniel Mandler 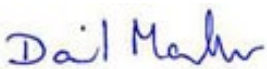 Date: 17.4.2024

German Principal Investigator(s):

Andrea Schaefer  Date: 15.5.2024

Abstract: The original objectives of the proposal were: i) integrate nanotechnologies with electrochemical reactions in a composite membrane, ii) allow in-situ monitoring of micropollutants (MPs) in polluted or reused (treated) water, and iii) remove micropollutants effectively in water reuse.

The project involved three groups, one headed by Prof. Schäfer from Karlsruhe Institute of Technology (KIT) whereas the two Israeli groups were one from the Technion (Tech), headed by Prof. Raphael Semiat and Prof. Daniel Mandler from the Hebrew University (HUJI).

The division of work among partners was that the group in KIT worked mostly on the photocatalytic and electrochemical degradation of steroid hormone (SH) in a membrane reactor. Moreover, they scaled up the electrochemical filtration system from 2 to 20 cm^2, followed by an evaluation and optimization of its efficacy in SH micropollutant removal. The group at the Technion focused on Fenton-like oxidation processes for removing propoxur, a micro-pollutant compound, from synthetic reverse osmosis concentrate (ROC) solution. A hierarchical methodology for determining the electro-removal mechanisms of micropollutants with different properties was developed. The group at the Hebrew University studied the electrochemical degradation of nonyl-phenol, which is also a common micropollutant using a flow-through cell based also on carbon nanotubes (CNTs). Furthermore, the group has studied the electrochemical generation of reactive oxygen species (ROS) through the oxygen reduction reaction (ORR).

In spite of the difficult times due to the COVID-19 epidemic, the collaboration continued all the time and included mutual visits of the PIs and also a long-stay visit of a student from KIT at HUJI. A few publications came out of this project, a few more are under preparation. We believe that most if not all of the objectives were accomplished and we have definitely made significant progress in the integration of photocatalytical and electrochemical methods in flow-through membrane systems that are based on different materials.

Following are the summary of the project progress and detailed descriptions of the activities of the three groups:

Table 1. The project progress compared with the plan.

Milestone in the proposal	Timetable	Status	Comments
M.1. Construct a flow-through filtration cell (HUJI, TECH, KIT)	01.2021 - 12.2021	Finished	- A flow-through electrochemical filtration system was constructed - A commercial electrochemical cell was purchased and was used for the investigation of the protocol for electrochemical filtration experiment - A micro-electrochemical crossflow cell with membrane area of 2 cm^2 was designed and externally constructed
M.2. Investigate electro-Fenton (EF) and electro-adsorption of the target micro-pollutants (TECH, HUJI)	03.2021 - 12.2021	Finished	- The faradaic efficiency of H_2O_2 and OH radcials was studied by the ORR using different carbonaceous materials and different catalysts.
M.3. Select target micropollutants and develop analytical methodology for micropollutant degradation at single ng/L limit of detection (HUJI, TECH, KIT)	01.2021 - 12.2021	Finished	-An ultra-high-performance liquid chromatograph coupling with a flow scintillator analyzer (UHPLC-FSA) method was developed by Roman Lyubimenko for radiolabeled steroid hormones SHs analysis [1] -A combined method integrating UHPLC-FSA and liquid scintillation counting (LSC) was developed to differentiate the concurrent electrochemical adsorption and degradation processes during micropollutant removal
M.4. Understand and optimize the purification processes and the removal of the target micropollutants (HUJI, TECH, KIT)	06.2021 - 5.2022	Finished	- The electrochemistry of micropollutants on the CNTs membrane [2, 3] was examined to understand and optimize the process - The limiting factors of the micropollutant removal were determined at varying operational conditions
M.5. Evaluate the feasibility of the NME process by comparing the electro-Fenton with Fenton oxidation (TECH)	01.2022 - 12.2022	Finished	-Comparative experiments of MP model compound (PR) removal by Fenton- and electro-Fenton-based oxidation processes were conducted aimed at studying the effects of various parameters, including reaction time, pH, molar ratio of H_2O_2 to iron, PR concentration, and reverse osmosis concentrate composition
M.6. Model the reaction dynamic and compare with	01.2022 – 12.2023	Finished	The mechanism in terms of the predominant reactive species contributing to the micropollutant degradation was examined for the

photocatalytic processes for micropollutant degradation (KIT)			electrochemical and photocatalytic membrane process
M.7. Model and improve the NEM using COMSOL Multiphysics software (TECH)	03.2022 – 06.2023	Not Finished	- Insufficient experimental data within the time frame hindered the development of a validated mode
M.8. Design, construct and test of a scaled-up NEM system (HUJI, TECH, KIT)	10.2022 – 12.2023	Finished	The scaled-up system was upscaled from 2 to 20 cm^2 A 3D printed flow cell was designed and printed.
Final analyses and reporting (HUJI, TECH, KIT)	10.2023-04.2024	Finished	Submitted

1. SCIENTIFIC OR TECHNICAL RESULTS

Technion:

Abstract

A publication titled "Competitive Study of Homogeneous and Heterogeneous Fenton-like Flow-through Propoxur Oxidation in ROC Solution," which acknowledges the project, has been published in Water Science & Technology Journal in 2023. This paper presents an investigation into the effectiveness of homogeneous and heterogeneous Fenton-like oxidation processes for removing propoxur, a micro-pollutant compound, from synthetic reverse osmosis concentrate (ROC) solution. Two electrolytic cell configurations were examined: divided and undivided in both the cathode is a porous fiber felt cathode (GF), where in the latter, an ion exchange membrane separates the cell into anodic and cathodic compartments. A hierarchical methodology for determining the electro-removal mechanisms of micropollutants with different properties was developed, and a manuscript is currently under preparation. In this methodology, the electrochemical removal mechanisms of micropollutant compounds in both cell configurations were determined through the systematic elimination of specific mechanisms. This approach facilitated the delineation of the individual contributions of each mechanism, including direct and indirect anodic oxidation, oxidation by electro-generated hydrogen peroxide, adsorption onto GF

and/or ion exchange membrane, and electro-adsorption onto GF and/or ion exchange membrane. The impact of various conditions such as current density, catalyst dosage, and mixing rate on the removal of propoxur in the homogeneous electro-Fenton process (i.e., H_2O_2/Fe^{2+}) was investigated in both electrolytic cell configurations.

Body of report:

Published article: A publication acknowledging the project titled "Competitive Study of Homogeneous and Heterogeneous Fenton-like Flow-through Propoxur Oxidation in ROC Solution" was published in Water Science & Technology (Volume 87, Issue 11, 2023, 2890–2904). This paper presents an investigation into the efficacy of homogeneous and heterogeneous Fenton-like oxidation processes for removing propoxur (PR), a micro-pollutant compound, from a synthetic reverse osmosis concentrate (ROC) solution. A submerged ceramic membrane reactor operated in continuous mode was employed for the study. A newly synthesized amorphous heterogeneous catalyst, ferrihydrite (Fh), was characterized, revealing a layered porous structure of nanoparticles. The ceramic membrane demonstrated a rejection rate of over 99.6% for Fh, indicating its sustainability. While homogeneous catalysis (Fe^{3+}) showed superior activity in PR removal compared to Fh initially, increasing H_2O_2 and Fh concentrations at a constant molar ratio resulted in PR oxidation efficiencies equal to those catalyzed by Fe^{3+}. The ionic composition of the ROC solution hindered PR oxidation, but increased residence time improved removal efficiency up to 87% at 88 min. Overall, the study underscores the potential of heterogeneous Fenton-like processes catalyzed by Fh in continuous operation mode.

Electrolytic cell configuration: Two electrolytic cell configurations were studied: divided and undivided, both at a volume of 50 mL. Schematics of both are displayed in Figure 1. The undivided electrolytic cell is equipped with parallel electrodes, a DSA plate ($Ti/RuO_2/IrO_2$, Whizzo S&T, China) as the anode, and a porous graphite fiber felt (GF) as the cathode. The dimensions of the electrodes are 100 x 25 mm (L x W) with a thickness of 1.5 mm and a 6 mm gap between them. The electrodes are connected to a DC power supply (0–5 A, 0–30 V) that provides a constant current. The same electrode layout is used in the divided cell, where an ion exchange membrane (Nafion N-424, Ion Power Inc.) separates the cell into anodic and cathodic compartments. The electrolyte (200 mL) can circulate within the cell (batch mode) or be fed to the cell

(continuous mode, indicated by dashed lines in the Figure 1) using a pump. An air blower is used for air sparging, which is distributed through a porous stone.

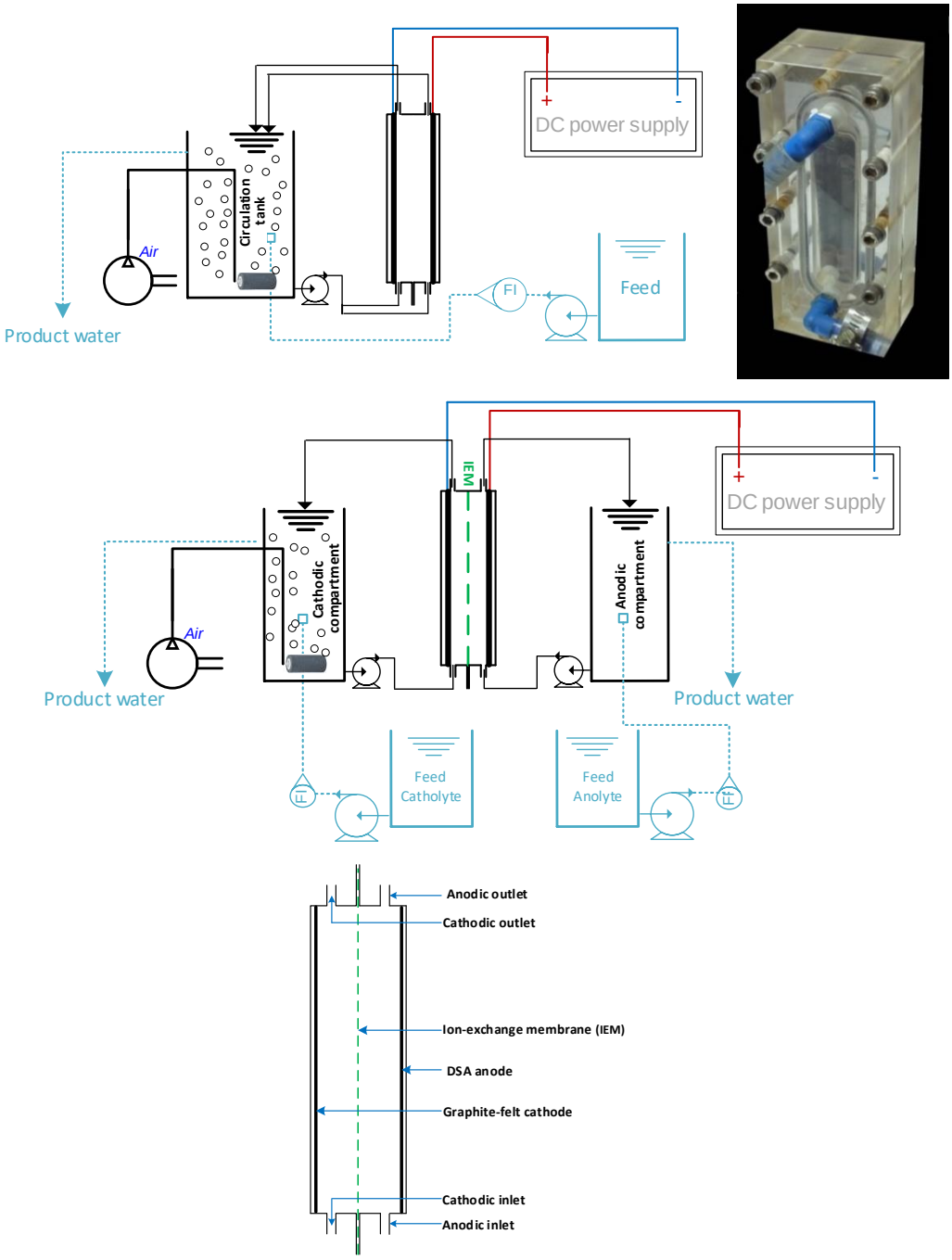

Figure 1. Schematics of the (a) undivided electrochemical systems including an image of the electrolytic cell; (b) undivided electrochemical system; (c) electrolytic cell. The difference between the divided and undivided cell is the ion exchange membrane (IEM), represented by the dashed green line

Development of a method for determining the electro-removal mechanisms of MPs:

Publication titled "Development of a Hierarchical Methodology for Determining the Mechanisms of Micropollutant Electro-removal" is being prepared. In the developed

methodology, the electrochemical removal mechanisms of micropollutant (MP) compounds in both undivided and divided cells were determined through the systematic elimination of specific mechanisms. This approach enabled the delineation of the individual contributions of each mechanism, including direct and indirect anodic oxidation, oxidation by hydrogen peroxide, adsorption onto GF and/or ion exchange membrane, and electro-adsorption onto GF and/or ion exchange membrane.

For example, batch experiments revealed that there was no adsorption of PR onto the GF within 24 h when no current was applied. The observed 10.6% PR removal was attributed to the simultaneous occurrence of three mechanisms: anodic oxidation, electro-adsorption onto the GF, and anodic oxidation of the electro-generated H_2O_2. The inhibition of the anodic oxidation of H_2O_2 is achieved by preventing its generation through the addition of N_2+Na_2SO_3. The addition of KI, acting as a surface-bound hydroxyl radical scavenger, suppresses both ·OH and direct electron transfer oxidation processes, thereby inhibiting anodic oxidation. The combined addition of KI with N_2 and Na_2SO_3 suppresses both potential anodic and hydrogen peroxide reactions. In this example, by eliminating the anodic reactions, it was concluded that the predominant removal mechanism for PR was electro-adsorption onto the GF.

In the divided cell, adsorption/electro-adsorption onto the IEM may also contribute to the MPs removal mechanism. Close PR removals were obtained in the cathode and anode compartments with and without applying current (Figure 2). In the absence of applied current, 12% and 14% of PR were removed within 60 min at the anode and cathode compartments, respectively, indicating adsorption onto the IEM. At current density of 1 mA/cm^2, PR removal increased to 22% and 25% at the cathode and anode compartments, respectively. The electro-adsorption of the IEM is evaluated by subtracting the electro-adsorption of the GF and the adsorption of the IEM.

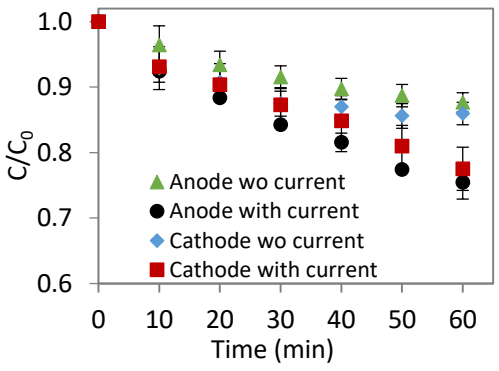

Figure 2. PR removal anode and cathode compartments without and with applied current (0.1 M Na_2SO_4, air purging, pH 3, 1.0 mA/cm^2)

In addition to the electrolytic cell configurations, the properties of the MPs affect their removal mechanism. Five pesticides, Parathion, Propoxur, Methomyl, Methamidophos, and Oxamyl- were studied, each exhibiting different properties such as the level of hydrophilicity and hydrophobicity, as shown in Figure 3a. Depending on the properties, MPs develop different types of mechanisms. For example, the compound charge is responsible for short-distance interactions with the GF and/or the ion-exchange membrane, as shown schematically in Figure 3b.

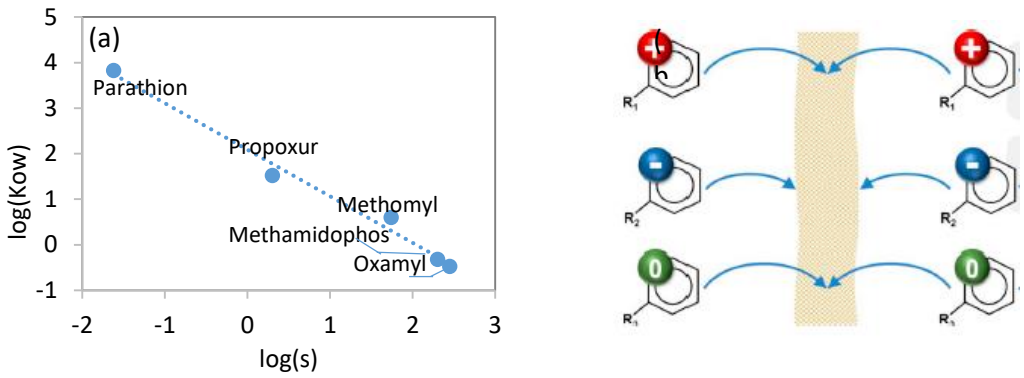

Figure 3. (a) Hydrophilicity and hydrophobicity of the tested MPs and (b) MPs adsorption onto IEM at a different compound charge

Parameter study: The homogenous electro-Fenton process (i.e., H_2O_2/Fe^{2+}) was studied at various conditions such as current density, catalyst dosage, and mixing rate for the removal of PR in both divided and undivided electrolytic cells. It should be noted that in the divided cell, emphasis was given to the cathodic compartment, where the catalytic oxidation process takes place.

In-situ production of H_2O_2 was measured in both divided and undivided cell configurations. Both electrolytic cell configurations demonstrated an increase in the H_2O_2 generation with the current density from 0.28 to 1.01 mA/cm^2 until reaching a relatively narrow plateau up to 1.40 mA/cm^2. Subsequently, a further increase in current density up to 2.13 mA/cm^2 led to a decrease in the H_2O_2 generation (Figure 4a). This may be attributed to the enhancement of H_2O_2 decomposition in the bulk solution and on the anode surface, as well as to the higher selective of 4e$^-$ ORR reaction. Electro-production of H_2O_2 in the divided cell was four times higher than that in the undivided cell probably due to anodic decomposition of the H_2O_2.

As seen in Figure 4b, PR removal increased as the current density was raised, corresponding to the enhanced electro-generation of H_2O_2 (Figure 4a). However, a subsequent increase in the current density resulted in diminished PR removal, consistent with the reduced generation of H_2O_2. PR removal in the divided cell was 1.6 times higher than that in the undivided cell. Divided electrolytic cells achieve higher reaction rates due to the elimination of side reactions that occur on the anode.

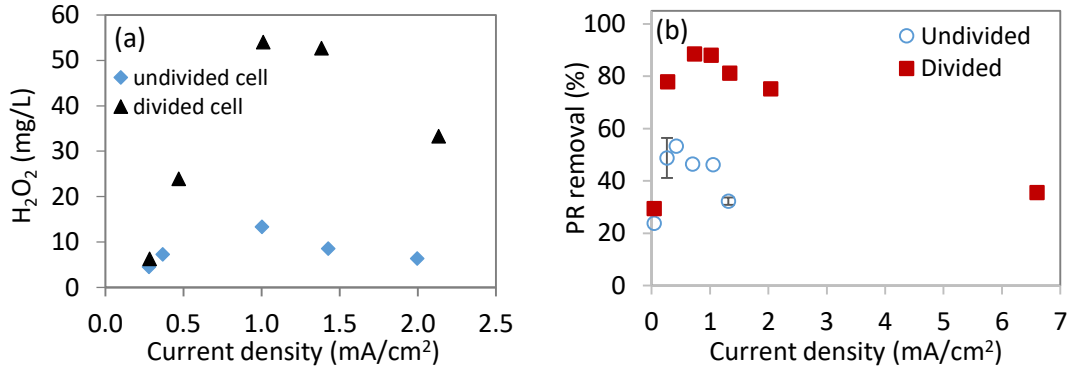

Figure 4. (a) H_2O_2 electro-generation and (b) catalytic PR removal in the divided and undivided electrolytic cells as a function of the current density (0.1 M Na_2SO_4, air purging, pH 3, 17.9 μM Fe^{2+}, 60 min reaction)

The effect of catalyst dosage was evaluated in the range from 0 to 40 μM Fe^{2+}. In both cell configurations, an increase in the Fe^{2+} concentration resulted in enhanced removal of the PR, as displayed in Figure 5. At a concentration of 40 μM Fe^{2+}, 96% of PR was removed within 40 min. The increase in Fe^{2+} concentration leads to higher concentrations of hydroxyl radicals, manifested by higher removal efficiency.

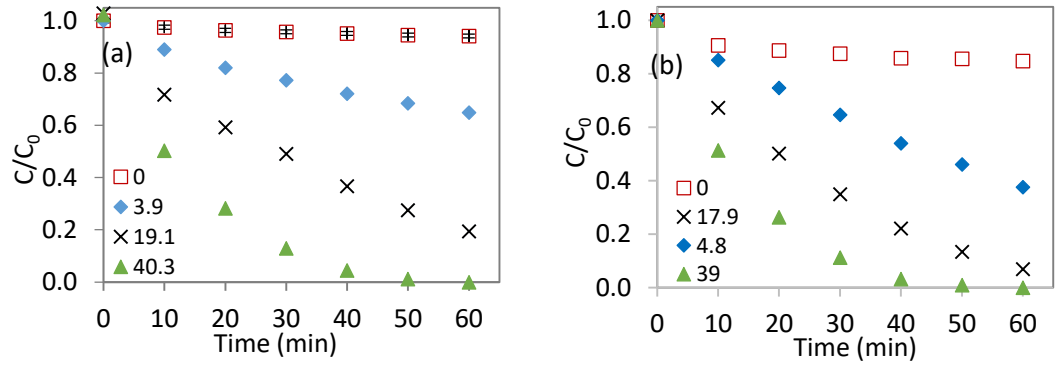

Figure 5. Catalytic removal of PR in the (a) undivided and (b) divided electrolytic cells as a function of the catalyst (Fe^{2+}) μM concentration (0.1 M Na_2SO_4, air purging, pH 3, 0.3 mA/cm^2, 60 min reaction)

As mixing can affect both the mass transfer between the MP compound and the electrodes and the current density, experiments were conducted at a constant current

density of 0.3 mA/cm². The results are displayed in Figure 6. An improvement in PR removal efficiency was observed by increasing the mixing rate from 50 to 100 mL/min. Further increase to 150 mL/min resulted in a slight increase. The superior performance of the undivided cell is evident in all mixing rates.

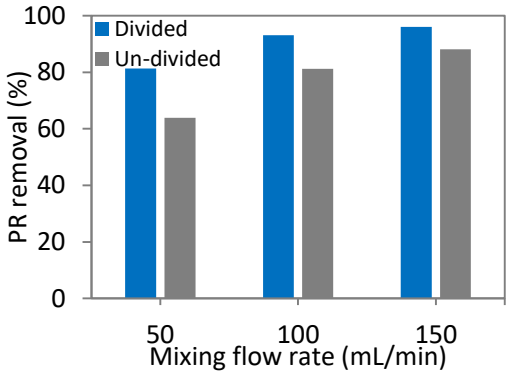

Figure 6. Catalytic removal of PR in the undivided and divided electrolytic cells as a function of the mixing rate (0.1 M Na_2SO_4, air purging, pH 3, 0.3 mA/cm^2, 17.9 μM Fe^{2+}, 60 min reaction)

HUJI

Abstract

The main objective of this project was to design a new electrochemical membrane cell for both monitoring and removal of micropollutants (MPs) in reused water. The first part of the work involved the application of a CNT-based flow-through system for the detection and removal of a common micropollutant, i.e., 4-nonylphenol (4-NP). This part has been successfully completed and summarized in a manuscript. A few versions or larger flow-through electrochemical cells were designed including a version that was 3D printed. We continued working on other MPs including carbamazepine (CBZ) and perfluoroalkyl substances (PFAS). This required the development of electrochemical systems for the efficient generation of ·OH radicals. We have studied the oxygen reduction reaction (ORR) using various carbon-based electrodes, such as carbon felt, carbon sponge, and CNTs. The faradaic efficiency of the formation of H_2O_2 and that of ·OH was determined. Different catalysts were examined and attached to the electrode surface. This resulted also in another manuscript. We found that the faradaic efficiency of the reduction of H2O2 using

CNTs on which a porphyrin catalyst was adsorbed was relatively very high, whereas the ORR resulted in low efficiency in the formation of ·OH radicals.

Methodology

HUJI was involved mostly in four tasks. **Task 1** comprised the construction of a flow-through electrochemical membrane, NEM, based on activated AC and CNTs in different configurations and adapting the state-of-the-art membrane filtration cell to electrochemical operation.

The heart of the flow-through system is the water flowing through the membrane under applied potential or current. This requires that, on one hand, high fluxes will be able to flow under moderate pressure and, on the other hand, the residence time (i.e., the time that the water is subject to the electrochemical potential) will be sufficiently high and that the diffusion layer will enable contact of the solutes with the electrode within this residence time. We took advantage of the high surface area, adsorption capacity, high conductivity, and nanometric structure of the CNTs.

Initially, we worked on a mini-scale, which means a surface area <4 cm^2 (Figure 7). As the counter electrode, we will use a stainless steel grid or a conductive Si ring. A three-electrode system, where the reference electrode (Ag/AgCl wire) was installed downstream. The potential window of the membranes was characterized and their stability was inspected by microscopy. Furthermore, analyzing the composition of the inlet and outlet water after flowing copious water was carried out.

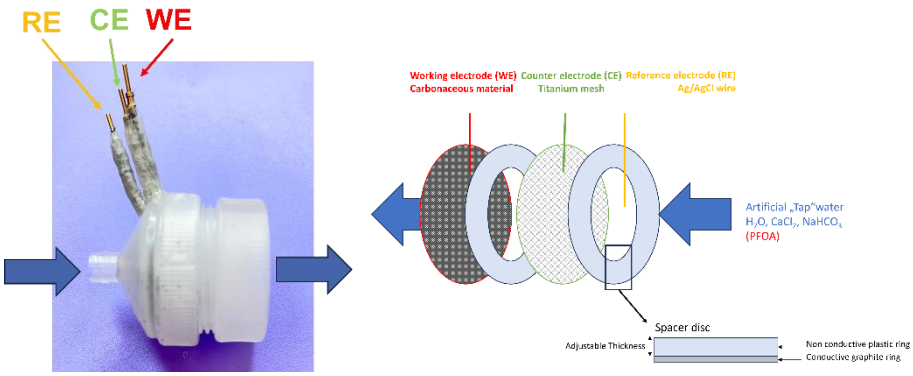

Figure 7: The electrochemical flow-through cell (left) and its scheme (right).

Task 2 involved the investigation of the removal processes of organic micropollutants by the NanoElectroMembrane (NEM). The research examined the decomposition of

the target compounds using a direct oxidation approach as well as the electro-Fenton approach or the accumulation of them while flowing through the NEM. The removal of the compounds was determined either electrochemically or by HPLC. We studied the effect of the applied potential, flow rate, concentration and type of electrochemical membrane on the removal efficiency.

Task 3 focused on developing electrochemical protocols for monitoring the micropollutants by the NEM. We have already shown that flow-through electrochemical cells based on CNTs can be used for the very sensitive detection of metals and organic species. Similar approaches were applied here. More specifically, we studied the adsorption of a few model compounds, such as nonylphenol and its electrochemical oxidation on CNTs. The various parameters affecting the sensitivity and selectivity of the detection were studied and optimized. Finally, we were also involved in Task 7, which aimed at upscaling the NEM system to a demonstration stage (electrode surface <40 cm^2).

Results

The electrochemical detection and removal of the micropollutant 4-nonylphenol (4-NP) As a model system we chose 4-NP as a micropollutant. To successfully develop an electrochemical approach for the detection of 4-NP in recycled water, it is necessary to meet the EU or EPA regulations, which means to enable the detection of 1 ppb of 4-NP, i.e., 4.54×10^{-9} M. Figure 8 shows the CV of 10^{-6} M 4-NP using a GCE carried out in a static three-electrode cell (Figure 1A) and a CNT based flow-through cell (Figure 1B). While a very small oxidation wave can be seen with the GCE, a clear irreversible oxidation peak is observed at 0.6 V with the flow-through cell. The peak is associated with the oxidation of 4-NP and is in agreement with previous studies.

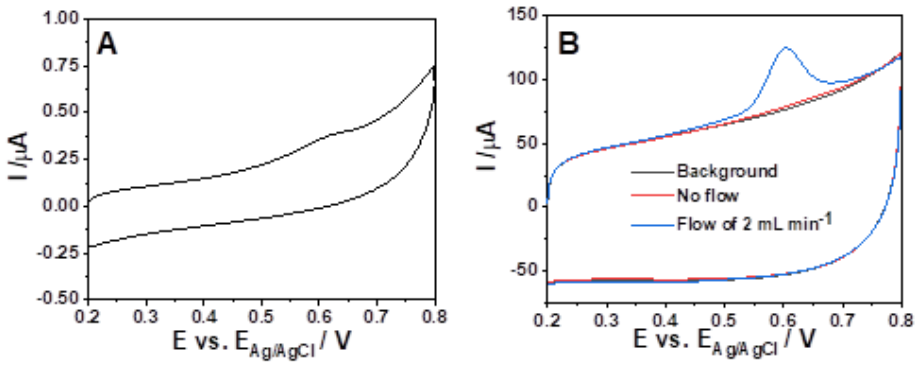

Figure 8– CV in a 10^{-6} M 4-NP and 0.1 M PBS pH 7.0 using: A) a GCE in a static cell; B) A CNT-based membrane in a flow-through cell: only buffer (black), 10-6 M 4-NP with

no flow (red) and the same concentration of 4-NP but with 2 mL min^{-1}. The scan rate was 0.1 V s^{-1}.

Next, we examined the performance of the CNT-based membrane under flow. Figure 9 shows the oxidation peak current measured after a volume of a 0.45 mM 4-NP (and 0.1 M PBS pH 7.0) solution flowed through the CNT membrane. The areal mass of the CT-50 CNTs was 0.12 mg cm^{-2}. It can be seen that a linear dependence is obtained between the volume of solution that passed through the membrane and the peak current, which implies that the adsorption sites for 4-NP on the CNT membrane were not saturated even after flowing 8 mL of 0.45 mM 4-NP.

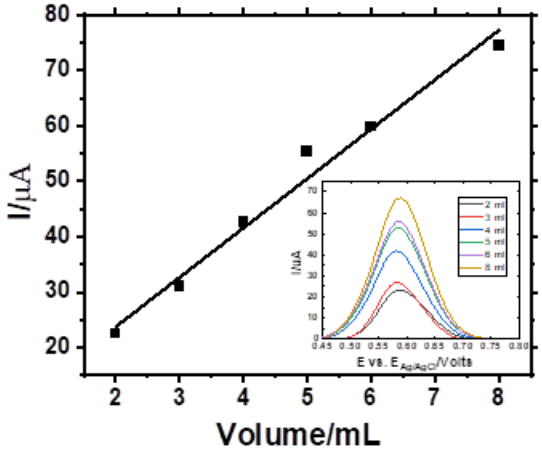

Figure 9: The oxidation peak current of 4-NP recorded with a CT-50 CNT-based membrane (0.12 mg cm^{-2}) as a function of a volume of 0.45 mM 4-NP (0.1 M PBS pH 7.0) solution flowed through the cell.

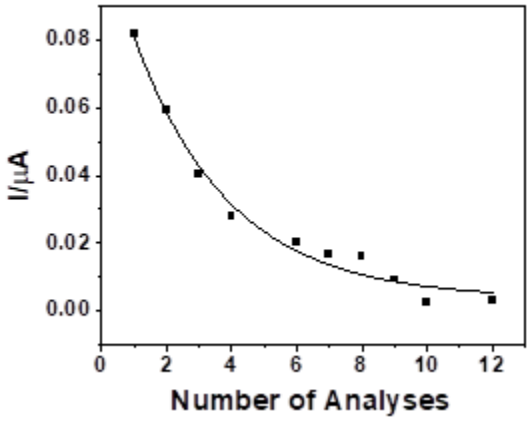

Figure 10: LSV oxidation peak currents recorded in a $4.5x10^{-7}$ M 4-NP and 0.1 M PBS (pH 7.0) solution as a function of the number of measurements. 4 mL of solution flowed at a rate of 2 mL min^{-1} through the flow-through cell before each measurement was performed.

Figure 10 shows the decrease in the oxidation peak current (measured by LSV) of $4.5x10^{-7}$ M 4-NP (0.1 M PBS pH 7.0) upon repeating the measurements without

replacing the CNT electrode. 4 mL of the solution flowed (2 mL min^{-1}) through the cell before each measurement was carried out. As previously reported, the electrochemical oxidation of phenols, and 4-nonylphenol as well, creates a polymeric film that fouls the electrode surface. The latter is not fully blocked; however, it becomes less sensitive to the 4-NP and obviously cannot be used for analytical purposes.

Figure 11 shows SEM images of the CNT membrane before and after carrying multiple analyses of 1 □M of 4-NP. Fouling of the CNT membrane by a carbonaceous material is evident, which is also expressed by the need to increase the pressure of the pump to keep the flow rate constant.

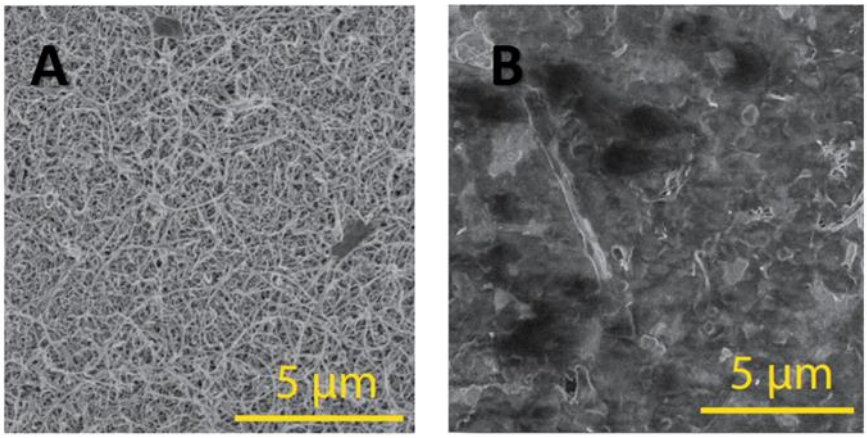

Figure 11: SEM images of the CNT membrane: A – before and B – after repeated analysis of 1 µM of 4-NP in 0.1 M PBS pH 7.0 using the flow-through cell.

Since it is not practical to replace the CNT membrane after every analysis, we carried out a set of experiments in which we applied a pulse of 10 s to the electrode with different potentials after every analysis. Figure 12 shows the LSV of 4-NP recorded after 1 mL of $4.5x10^{-7}$ M and 0.1 M PBS pH 7.0 flowed through the cell using the same CNT membrane. After the LSV and before another volume of solution flowed through the cell, the cleaning process of a potential pulse was applied. The red line in Figure 5A shows the signal of 4-NP obtained on a clean and new CNT membrane. It can be seen that the application of −0.6 V did not fully recover the electrode and the anodic peak current kept decreasing after each analysis. Hence, we applied a more negative pulse of −1 V (Figure 5B), which prevented the oxidation peak to further decrease, yet, the current did not fully recover its initial value. A pulse of −2 V (Figure 5C) on the other hand, caused the peak current to almost attain its initial value even after 12 consecutive analyses. This cleaning process did not add any complications and enabled us to repeatedly use the same CNT membrane.

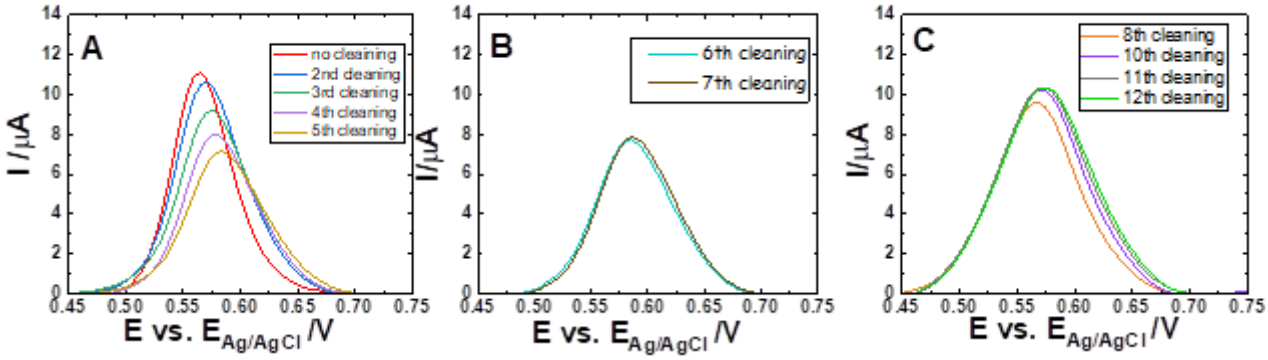

Figure 12: Cleaning the CNT membrane by a short potential pulse. Repeated LSVs of a CNT membrane, which was pulsed for 10 s at different potentials before flowing 1 mL of 4.5×10^{-7} M 4-NP and 0.1 M PBS pH 7.0 solution. A – −0.6 V; B – −1 V; C – −2 V.

This led us to form a calibration curve that is shown in Figure 13. The solutions with known concentrations of 4-NP flowed through the cell with a rate of 2 mL min^{-1} and LSV (0.5 V s^{-1}) was carried out after 2 mL of solution passed the CNT membrane (0.12 mg cm^{-2}). The 50 Hz noise of the grid was removed, which yielded very high sensitivity. The curve could be even further extended to 10^{-10} M, spanning three orders of concentration magnitude; however, the slope changed. The LOD for the system is $1.92 \cdot 10^{-10}$ M (equals 42.3 ppt) of 4-NP after 50 Hz filtration. This is well below the EU or EPA regulations and therefore, with some adaptation, this approach could be used for monitoring the levels of this micropollutant.

The next step was to combine electrochemical treatment and monitoring with the same flow-through electrochemical cell. Namely, as the water flows through the CNT membrane, applying a constant potential is likely to oxidize and remove the 4-NP, and the levels of the micropollutant could be determined in the same cell either with the same electrode or more likely with an additional working electrode. Therefore, we initially flowed the CNT membrane with a solution of 4.5×10^{-5} M 4-NP while applying different constant potentials. The outlet stream was collected and analyzed electrochemically using a GCE. Table 1 shows the removal percentage of the 4-NP.

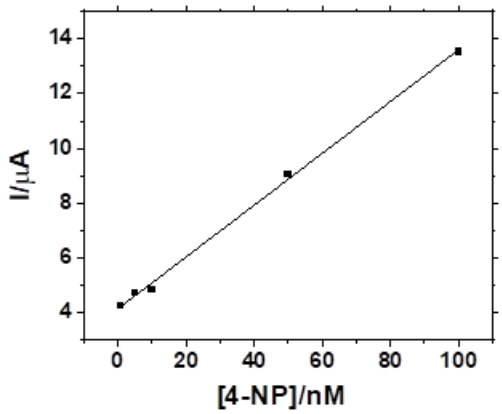

Figure 13: Calibration curve 4-NP in 0.1 M phosphate buffer, pH 7. The scan rate was 0.5 V s^{-1}.

Table 1: the removal percent of 4-NP (initial concentration was 45 mM) by applying different constant potentials and a rate of 2 mL min^{-1}.

Applied potential	Outlet [4-NP]/μM	Removal %
0.3	8.67	81
0.6	1.5	97
0.7	2.87	94
1.0	0.02	99

It can be seen that as the potential applied reaches the oxidation potential of 4-NP a significant decrease is detected in the concentration of the micropollutant in the outlet effluent. A potential of 1.0 V removes almost all the 4-NP, which suggests that the residence time of the micropollutant in the CNT membrane is sufficient for all molecules to be within electron transfer distance from the CNT.

This paved the way for the last step, i.e., removal and monitoring. To accomplish this challenge we 3-D printed a flow-through cell (Figure 14) where another CNT-membrane was added and used upstream for the detection of the levels of 4-NP in the effluent after the electrochemical treatment.

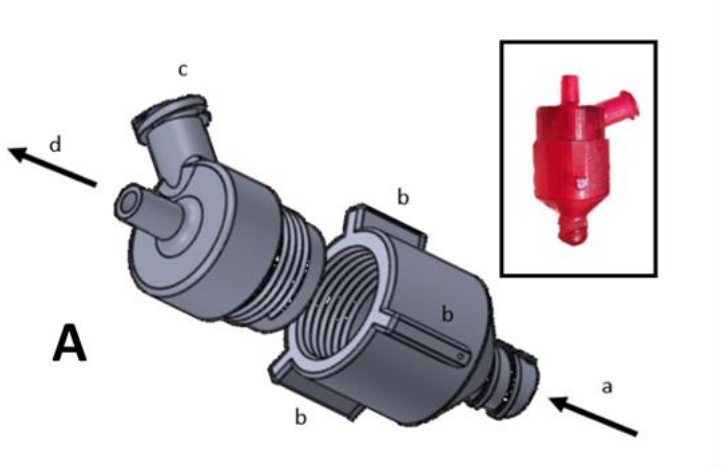

Figure 14: A – Schematics of the 3-D printed flow-through electrochemical cell; B – schematics of the cross-section of the cell.

Electrochemical generation of reactive oxygen species (ROS) on a flow-through membrane. Our approach has involved the electro-Fenton (EF) reaction that is based on the oxygen reduction reaction (ORR) to generate H_2O_2. The latter is further reduced to form ·OH radicals (eq. 1-2).

(eq. 1) $$O_2 + 2e^- + 2H^+ \rightarrow H_2O_2$$

(eq. 2) $$H_2O_2 + e^- \xrightarrow{\text{Catalyst}} \cdot OH + OH^-$$

We started by searching for catalysts for our flow system. As can be seen in Figure 15, the ORR is evident, and the response depends both on the carbonaceous material as well as on the adsorption of different catalysts.

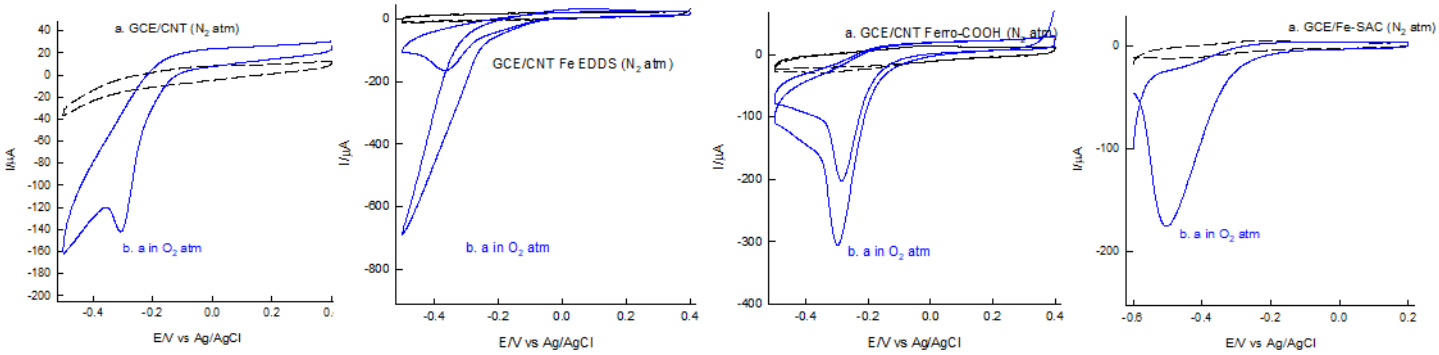

Figure 15: Cyclic voltammetry in the absence (black curves) and presence (blue curves) of oxygen using: A – glassy carbon electrode (GCE) coated with carbon nanotubes (CNT); B – CGE/CNT with Fe-EDDS; C – Ferrocene and D – Fe single-atom catalyst.

Yet, while the faradaic efficiency of the formation of H_2O_2 can be very high, that of the $^{\cdot}OH$ formation is usually below 1% (Figure 16) and most efforts are directed towards the development of efficient catalysts.

Among the catalysts that we have been using are inorganic complexes such as CoTPP (cobalt(II) tetraphenylporphyrin) and single-atom catalysts (SACs) that are attached to a carbonaceous electrode surface. Our group has started a collaboration with the Department for Chemistry at Bar-Ilan University. This group synthesizes carbon-supported SACs for the electro-Fenton reaction. The group at

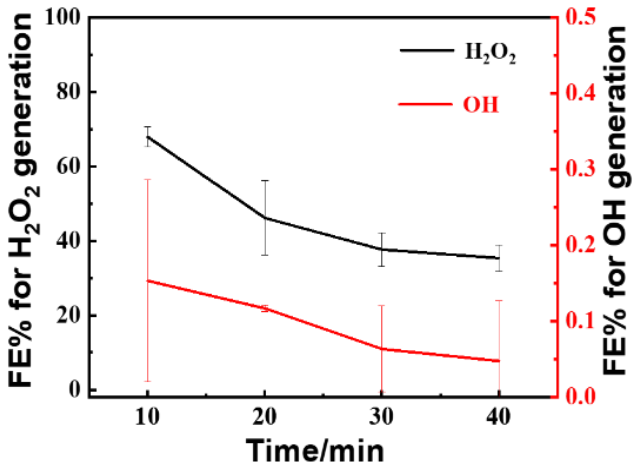

Figure 16: The faradaic efficiency of the formation of H_2O_2 and $^{\cdot}OH$ as a function of time on a carbonaceous electrode.

the Hebrew University is responsible for measuring the ability of these catalysts to improve the production of hydroxyl radicals and introduce the catalyst to the flow system.

Our initial experiments were conducted in a static cell and then we switched to a flow system, which was recently modified. The flow system can be used as a dual detection and removal device. Yet, we observed that the removal of the 4-NP that is achieved by electrochemical oxidation results in fouling of the membrane. Therefore a new system whereby two membrane electrodes are used; one for the removal and the other for the detection has been assembled by 3D printing. Figure 17 shows the faradaic efficiencies of hydrogen peroxide and hydroxyl radical formation as a function of time using different catalysts, which were synthesized at Ben Gurion University by Menny Shalom's group.

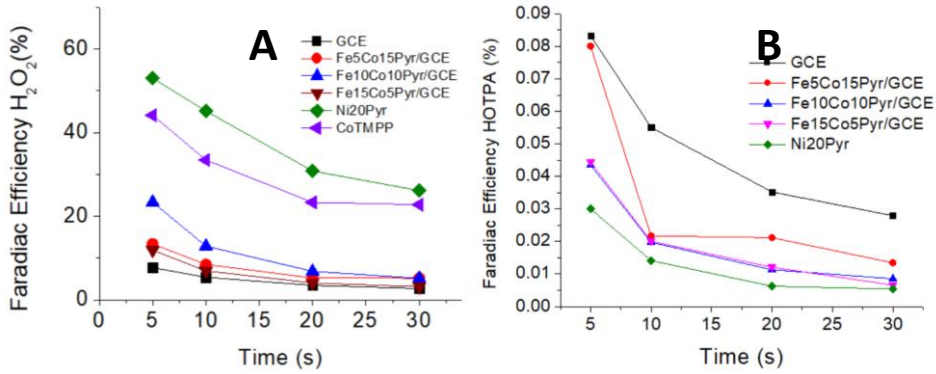

Figure 17: The faradaic efficiency of: A – H_2O_2 and B – $^{\cdot}OH$ radicals as a function of time using different catalysts.

Again, it can be seen that we still have not achieved good efficiency for the radical formation. Therefore, we are currently studying the reduction of H_2O_2 in the absence of oxygen (eq. 3).

(eq. 3) $$H_2O_2 + e^- \xrightarrow{\text{Catalyst}} {}^{\cdot}OH + OH^-$$

Figure 18 shows that indeed $^{\cdot}OH$ is formed with a faradaic efficiency of ca. 1%. This is too low and we are working now trying to improve it. It should be noted that this is still without a catalyst, yet, and based on the results above, we might need to modify the current catalysts that we are using.

One of the parameters that we are planning to change is the type of the CNTs that we apply. At present, we use MWCNTs and it seems that ORR performs much better on SWCNTs. The type of CNTs affects also the ability to form stand-alone membranes, which we make by filtering a dispersion of CNTs through a PVDF filter. MWCNTs are very difficult to separate from the support.

Figure 18: The faradaic efficiency of ·OH formation by the electrochemical reduction of H_2O_2

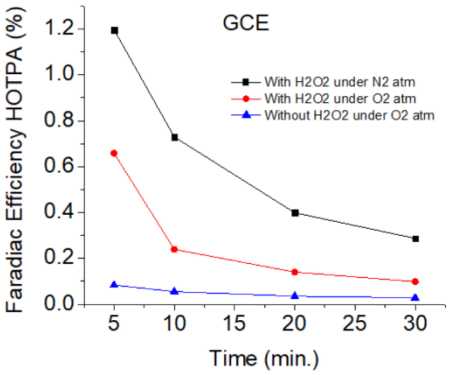

As mentioned above, we also employ inorganic complexes, such as CoTPP (Figure 5A), which is easily adsorbed on a carbonaceous material (Figure 19B). Figure 6 shows the faradaic efficiency of H_2O_2 and OH formation before and after adding the CoTPP. It can be seen that both efficiencies have increased as a result of introducing the cobalt complex.

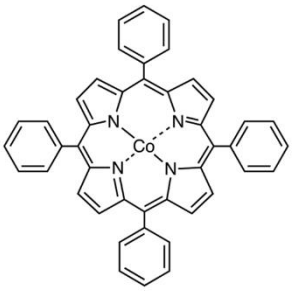

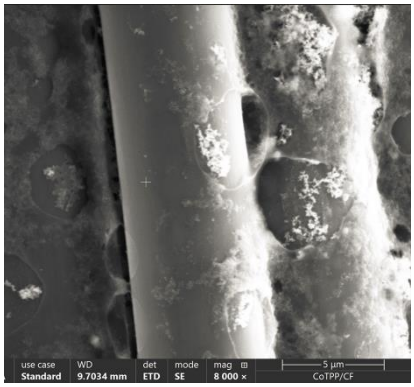

Figure 19: A – The structure of CoTPP, B – SEM image of CoTPP adsorbed on a carbon fabric used as an electrode in a flow

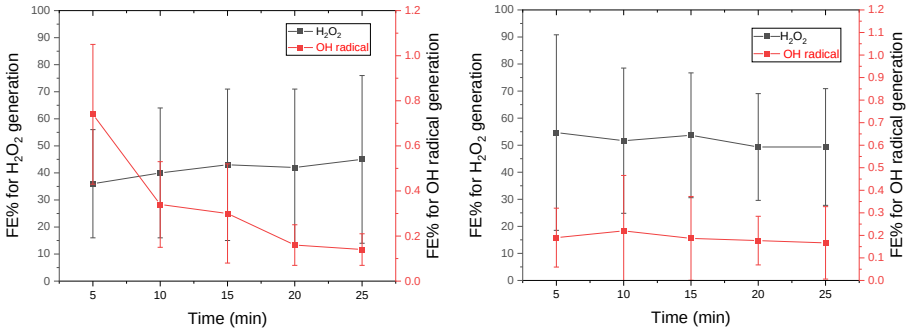

Figure 20: Faradaic efficiency of H_2O_2 and ·OH generation before (A) and after (B) adding CoTPP to a carbonaceous electrode.

To summarize, in spite of the difficulties during the project, i.e., COVID-19 and at the end the events in Israel, we have made substantial progress. We are still summarizing some of the results in a few manuscripts but we are already looking forward to the next step in our collaboration with KIT.

KIT

Abstract

The main objectives of the German subproject include i) The design and construction of a micro-electrochemical flow-through cell, featuring a membrane area of 2 cm^2. This setup is intended for a comparative analysis with photocatalytic processes in steroid hormone (SH) micropollutant removal, highlighting advantages in throughput and cost-effectiveness. ii) Investigation of the electrochemical degradation dynamics of SH micropollutants under various operational conditions, employing a carbon nanotube (CNTs) ultrafiltration membrane supplied by David Jassby at UCLA, US. and iii) Examination of the underlying mechanisms governing both electrochemical and photocatalytic degradation of SH micropollutants. iv) The scale-up of the electrochemical filtration system from 2 to 20 cm^2, followed by an evaluation of its efficacy in SH micropollutant removal.

Methodology

<u>1) Establishment of the micro-electrochemical flow-through system</u>

A custom-designed micro-electrochemical flow-through cell, featuring a 2 cm^2 membrane area, was developed and its construction outsourced. This innovation aims

to facilitate the study of electrochemical degradation dynamics and enable a comparative analysis with photocatalytic membrane processes for micropollutant removal, focusing on smaller scale operations for enhanced throughput and reduced experimental costs. Figure 21 presents the schematic diagram of the electro-filtration reactor.

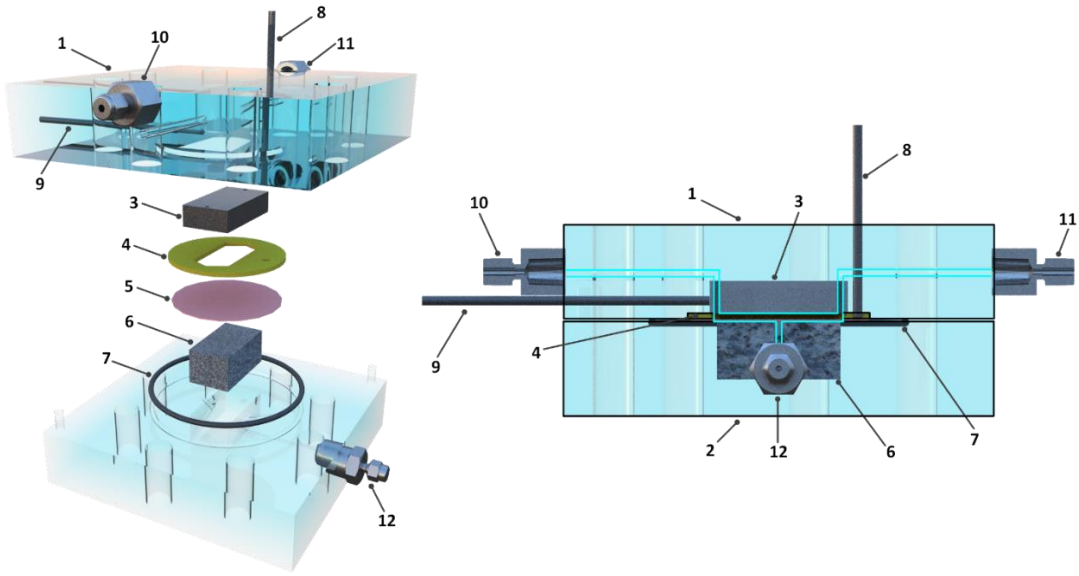

Figure 21. Schematic diagram of (Left) the exploded view, and (Right) side view of the electrochemical membrane reactor with a membrane area of 2 cm^2, 1 top cell, 2 bottom cell, 3 titanium cathode, 4 PEEK spacer, 5 electrochemical membrane, 6 titanium porous support, 7 O-ring, 8 platinum wire, 9 titanium wire, 10 feed inlet connector, 11 crossflow outlet connector, and 12 permeate outlet connector. Reprinted from [4].

The construction of the electrochemical filtration cell utilized acrylic material, incorporating a titanium sheet as the counter electrode to provide an effective electrochemical surface area of 2 cm^2. In assembling the electrochemical membrane, which functions as the anode, it was positioned above a porous support made from titanium particles (180-230 mesh). The membrane was compressed against a 0.8 mm thick polyether-ether-ketone (PEEK) spacer, strategically placed between the electrochemical membrane and the titanium cathode, to create a precisely sealed area of 2 cm^2. Platinum and titanium wires were integrated into the cell, serving as contact points for the electrochemical membrane anode and the titanium cathode, respectively.

The operating principle is to pressure water through the electro-filtration cell that contains a cathode, and an electro-membrane as anode with a constant flow rate of

feed solution using a peristaltic pump. An electric field will be applied for the system to control the cell voltage between the anode and cathode when performing the electro-filtration to remove SH micropollutants.

2) Scale-up of the electrochemical filtration system from 2 to 20 cm^2

A scaled-up electro-filtration system was designed and constructed, aiming to evaluate the performance of a variety of flat sheet electro-membranes, including ultra- and micro-filtration (UF and MF) electro-membranes, in SH micropollutants removal during water reuse processes with an extended membrane area. Configuration and flow diagram of the designed electro-filtration system are presented in Figure 22.

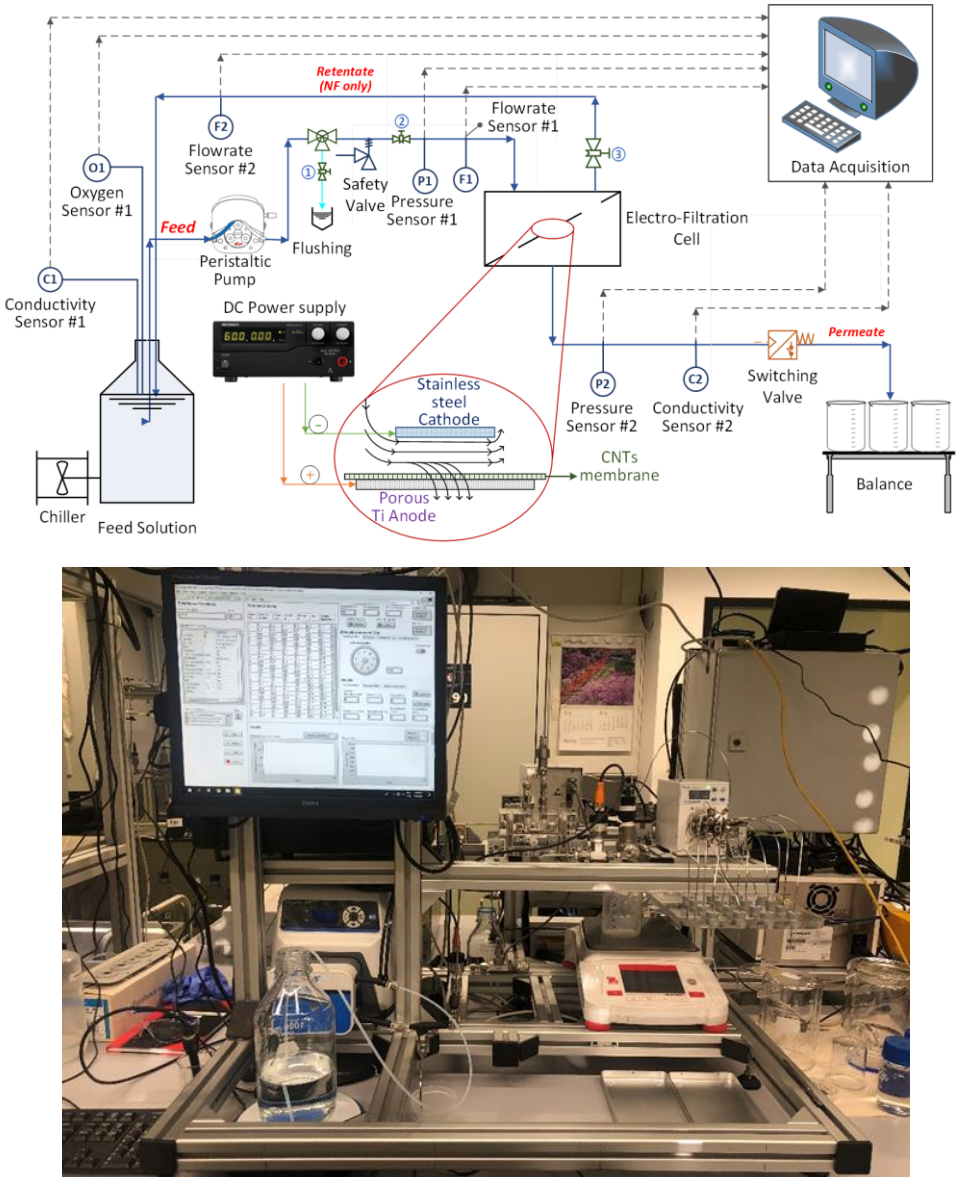

Figure 22. Schematic and picture of the established electro-filtration system. Reprinted from [4].

Central to this system is a commercial electrochemical filtration cell (Figure 23, model CF016A, SterliTech, USA [5]). This cell is designed to accommodate an electrochemical membrane as a flow-through anode, and a stainless steel plate as a cathode, providing an effective filtration area of 20 cm^2. Other key components of the setup include: a direct current power supply to regulate the voltage across the electrochemical cell, and a peristaltic pump that allows flow rate ranging from 0 to 92 mL/min, a 16-port switching valve, which facilitates the automatic collection of permeate samples, a balance is employed to measure the mass of the permeate, and a data acquisition card is used to acquire and transfer data from the various sensors and the balance to a computer for analysis. The operation of the peristaltic pump, power supply, and switching valve is integrated and automated through a LabView program interface (version 20.0.1, National Instruments, USA).

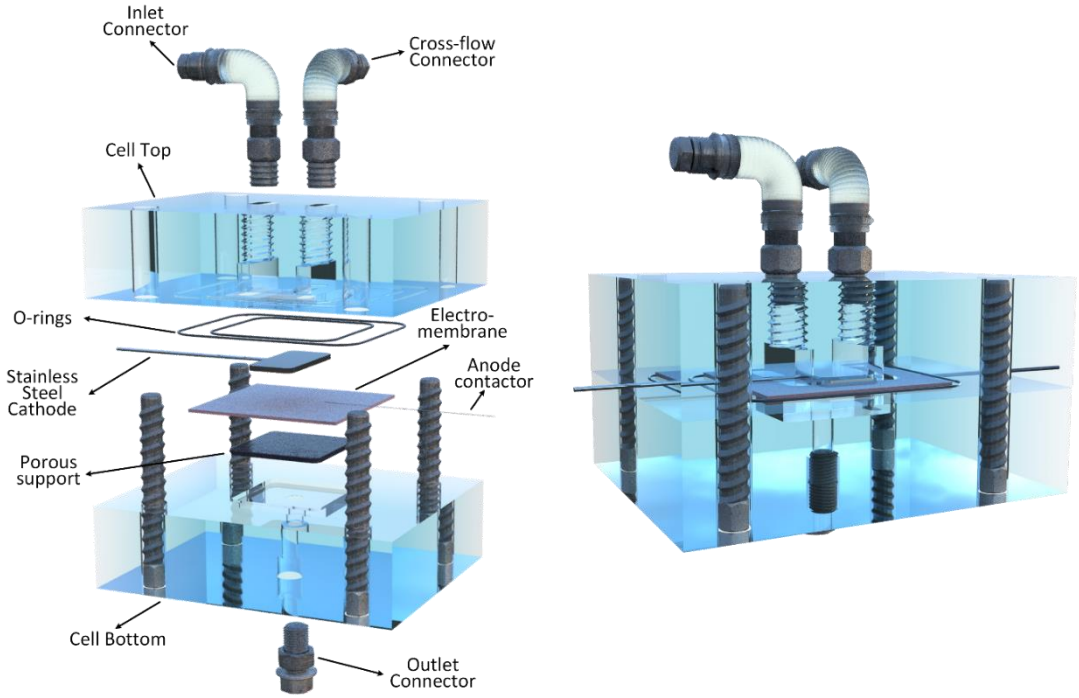

Figure 23. Schematic diagram of the electrochemical membrane reactor with membrane area of 20 cm^2. Reprinted from [6].

3) Development of analytical method for differentiation between electrochemical adsorption and degradation of SH micropollutant

An innovative methodological approach was developed, integrating a Liquid Scintillation Counter (LSC) and an Ultra High-Performance Liquid Chromatograph (UHPLC) coupled with a Flow Scintillator Analyzer (FSA), to unravel the mechanisms of SH removal by the EMR, focusing specifically on the simultaneous processes of

degradation and adsorption. The UHPLC-FSA method, adapted from Lyubimenko et al. [1], is deployed for high-resolution separation of sample constituents. This enables precise identification and quantification of both the intact SH compound and its degradation byproducts that may form within the system. Such separation is essential for a comprehensive understanding of the chemical behavior of SH during electrochemical reactions. In parallel, the LSC technique quantifies the total ^{3}H activity within the samples, providing an exhaustive assessment of all radiolabelled species present, whether they are the parent compound or its degradation products.

This synergistic application of advanced analytical techniques provides an in-depth insight into the complex chemical and physical reactions occurring within the electrochemical matrix, enhancing our understanding of the underlying mechanisms of the electro-filtraiton system.

Results

1) Degradation performance of the electrochemical membrane reactor for steroid hormone micropollutant

The electrochemical degradation of micropollutant with a carbon nanotube (CNTs) ultrafiltration membrane (provided by David Jassby at UCLA, US [2]) was examined at a cell voltage of 1.6 V and a flux of 600 L/m^{2}h (Figure 24), which demonstrated a remarkable removal over 98% (limited currently by analytical detection limit). This performance is particularly notable when compared to the photocatalytic membrane process utilizing a PES-TiO_2 membrane under UV irradiation, which reported a removal of 47±8% under the same flux and a significantly higher energy consumption (10 mW/cm^2) [7].

As illustrated in the chromatograms (Figure 24D), alongside the reduction in E2 concentration, three distinct byproducts were identified based on their unique retention times—approximately at 3, 5, and 8 minutes—utilizing UHPLC-FSA. The normalized ^{3}H concentration in the permeate was found to be in alignment with the combined concentrations of intact E2 and its three transformation products, as quantified by UHPLC-FSA, according to mass balance analysis. This evidence suggests that these three byproducts are the primary intermediates of E2 degradation within the CNT EMR (Figure 24C).

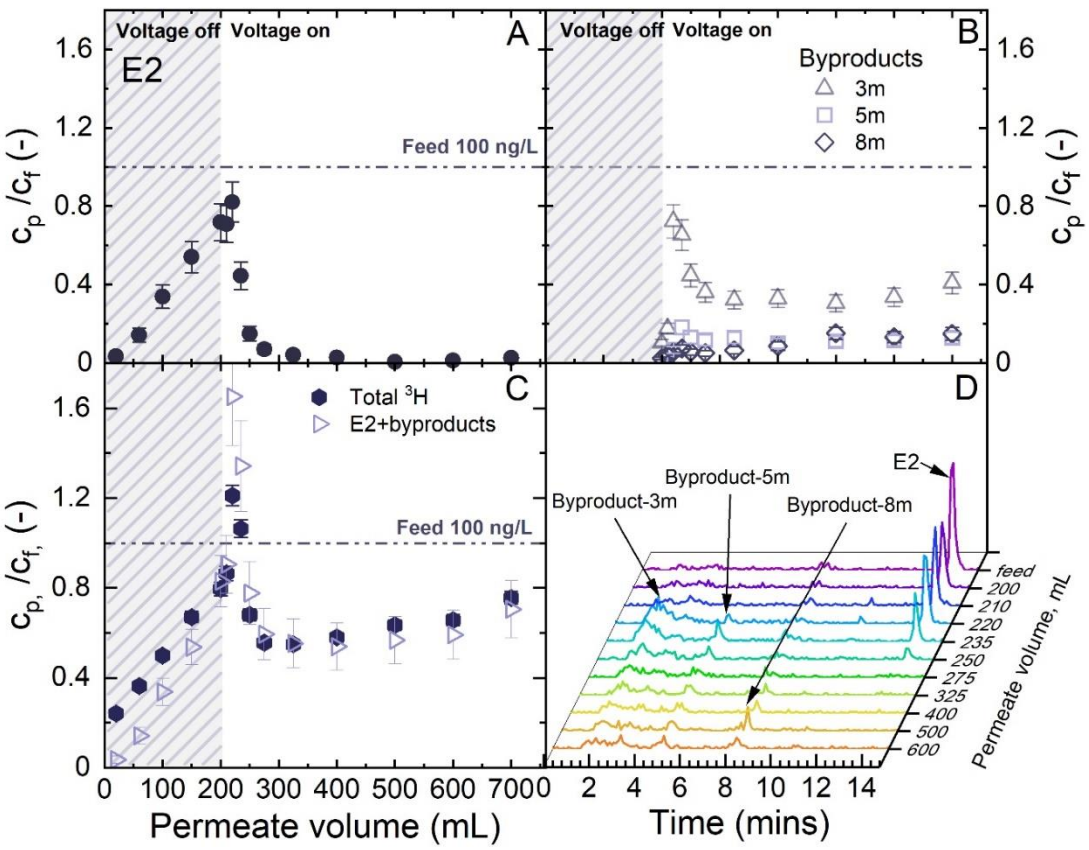

Figure 24. Electrochemical degradation of E2 within CNT EMR as normalized concentration of (A) E2 ($c_{p,E2}/c_{f,E2}$), (B) byproducts ($c_{p,met}/c_{f,met}$), (C) 3H, and the sum of E2 and the three byproducts vs. accumulated permeate volume, and (D) UHPLC-FSA chromatograms of E2 during the electrochemical degradation with increasing accumulated permeate volume. $c_{f,E2}$ = 100 ng/L, V_{cell} = 1.6 V, J_f = 600 L/m^{2}h (2 mL/min), 1 mM $NaHCO_3$, 10 mM NaCl, 27.2 mg/L EtOH, 79.2 mg/L MeOH, pH 8.2±0.2, 23±0.2 ℃. Reprinted from [4]

2) Limiting factors determined in the electrochemical membrane reactor

The limiting factors of the EMR were systematically identified across a range of operational conditions (cell voltage, flux, concentration), thereby providing deep insights into the mechanisms of EMR in the treatment of micropollutants.

Applied cell voltage determines the rate of electron transfer rate at the membrane surface. To delve deeper into the extent to which the rate of electron transfer could limit the electrochemical degradation of E2, experiments were conducted across a spectrum of cell voltages, ranging from 0.9 to 3 V (Figure 25).

When cell voltages of 0.9 V and 1.05 V were applied, the CNT EMR demonstrated relatively modest E2 removal of 13±10% and 22±8%, respectively (Figure 25A). A slight increase in voltage to 1.2 V—surpassing the critical potential required to initiate E2 electrooxidation, markedly improved E2 removal to 94±2%. Furthermore, at voltages

exceeding 1.2 V, E2 removal efficiency reached 99±1%, with the removal rate stabilizing at a plateau of approximately 5±0.3 mol/m²s. This plateau indicates a regime limited by surface concentration.

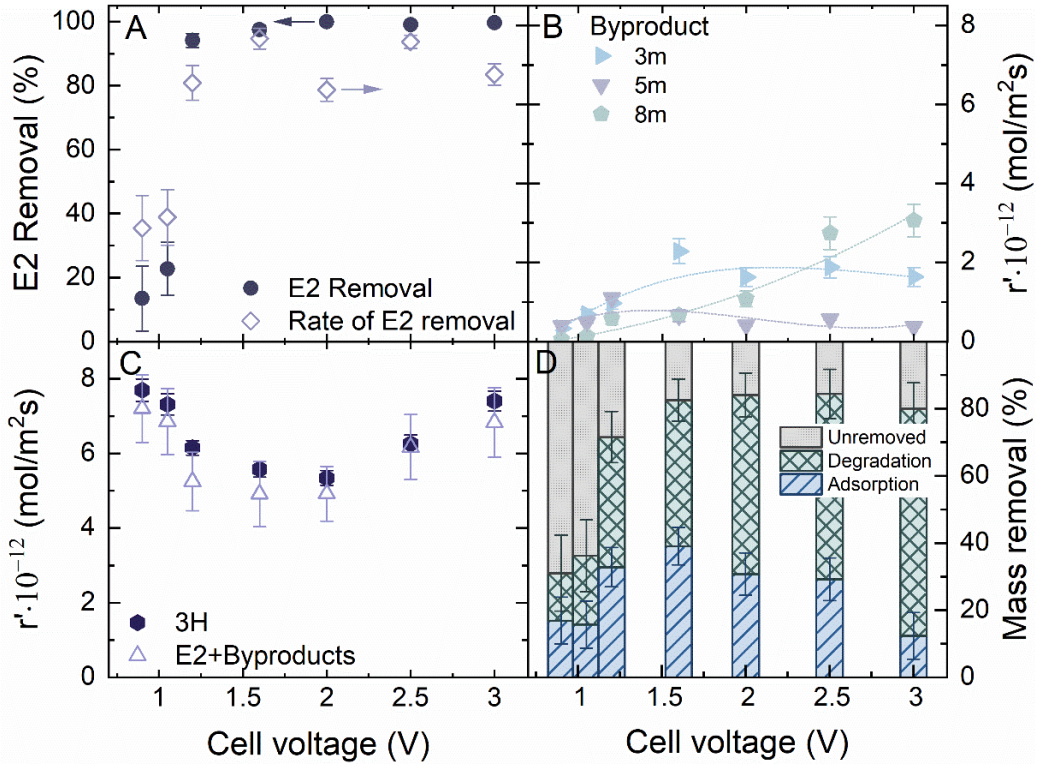

Figure 25. Impact of cell voltage on the electrochemical degradation of E2 expressed as (A) E2 removal and apparent rate of E2 removal, and (B) apparent rate of byproduct formation, (C) 3H, and the sum of E2 and the three byproducts in permeate; and (D) contribution to the mass removal of E2 by the electrochemical adsorption and degradation vs. cell voltage. $c_{f,E2}$ = 100 ng/L, J_f = 600 L/m²h (2 mL/min), 1 mM $NaHCO_3$, 10 mM NaCl, 27.2 mg/L EtOH, 79.2 mg/L MeOH, pH 8.2±0.2, 23±0.2 ℃. Reprinted from [4]

The hydraulic residence time (t_r) of micropollutants within the EMR is regulated by the water flux, which plays a crucial role in shaping the interaction dynamics between the micropollutants and the membrane. An extended hydraulic residence time enhances the likelihood of micropollutant molecules encountering and adsorbing onto the electron transfer sites on the membrane surface. To ascertain the flux threshold necessary to enter the hydraulic-residence-time-independent regime within the CNT-based EMR, a sequence of experiments was performed with water flux ranging from 60 to 3000 L/m²h (Figure 26). Correspondingly, the t_r was observed to decrease from $40 \cdot 10^{-3}$ to $0.8 \cdot 10^{-3}$ s within this range.

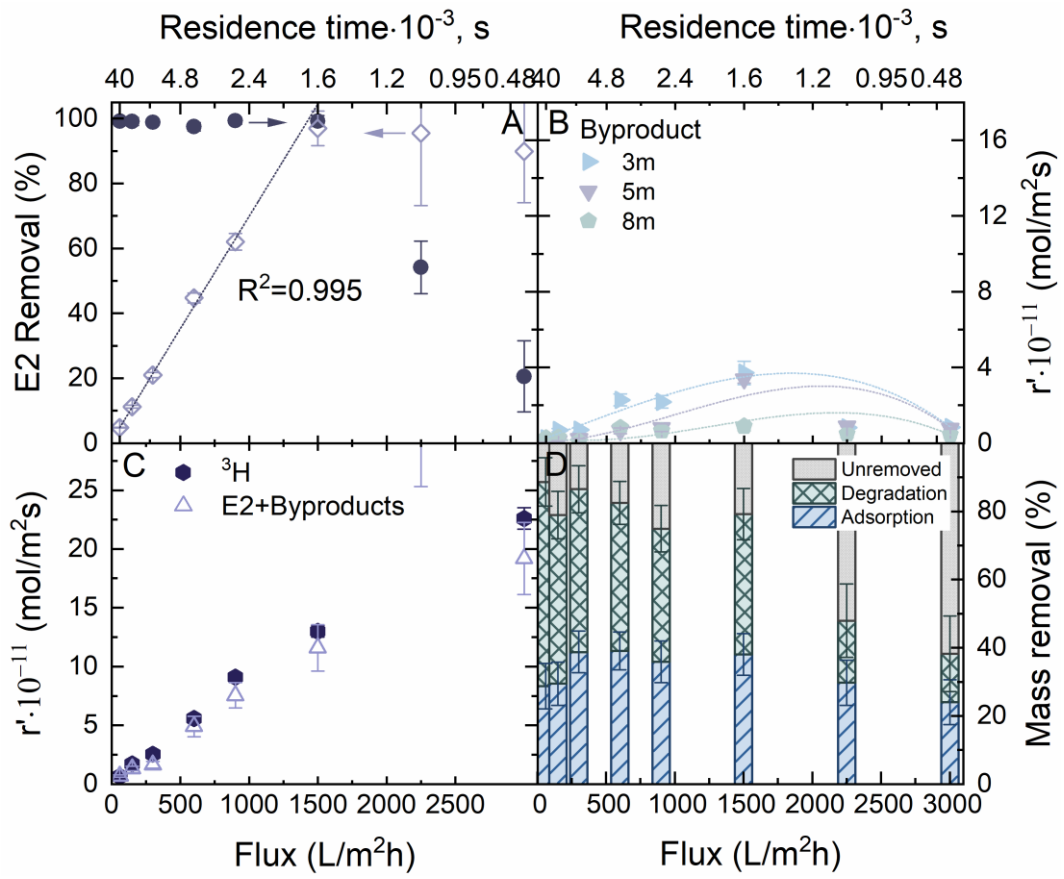

Figure 26. Impact of water flux on the electrochemical degradation of E2 expressed as (A) E2 removal and apparent rate of E2 removal, and (B) apparent rate of byproduct formation, (C) 3H, and the sum of E2 and the three byproducts in permeate; and (D) contribution to the mass removal of E2 by the electrochemical adsorption and degradation vs. flux. $c_{f,E2}$ = 100 ng/L, V_{cell} = 1.6 V, 1 mM $NaHCO_3$, 10 mM NaCl, 27.2 mg/L EtOH, 79.2 mg/L MeOH, pH 8.2±0.2, 23±0.2 °C. Reprinted from [4].

A robust linear correlation (R^2=0.995) was found between the shortening hydraulic residence time, from $39.6 \cdot 10^{-3}$ to $1.6 \cdot 10^{-3}$ s (corresponding to an increase in flux from 60 to 1500 L/m²h), and the rate of E2 removal. As the flux increased, the rate of E2 removal rose linearly from $(0.6 \pm 0.02) \cdot 10^{11}$ to $(12 \pm 0.6) \cdot 10^{11}$. This suggests that at hydraulic residence times less than $1.6 \cdot 10^{-3}$ s, the kinetics of the electrochemical reaction were constrained by the availability of E2 molecules within the EMR per unit time. Upon further increasing the flux to 3000 L/m²h, the rate of E2 removal reached a plateau, indicating a shift to an electron-transfer-limited regime. In this regime, the rate of the electrochemical reaction is insufficient to regenerate the CNT membrane surface for additional adsorption. The pronounced transition from mass-limited to

electron-transfer-limited regimes can be attributed to the direct electron transfer mechanism's strong reliance on the availability of electrochemical sites.

To explore the possibility that the degradation kinetics of E2 within the EMR are influenced by its initial concentration, electrochemical filtration experiments were conducted across a range of E2 concentrations, from 50 to 10^6 ng/L (Figure 27).

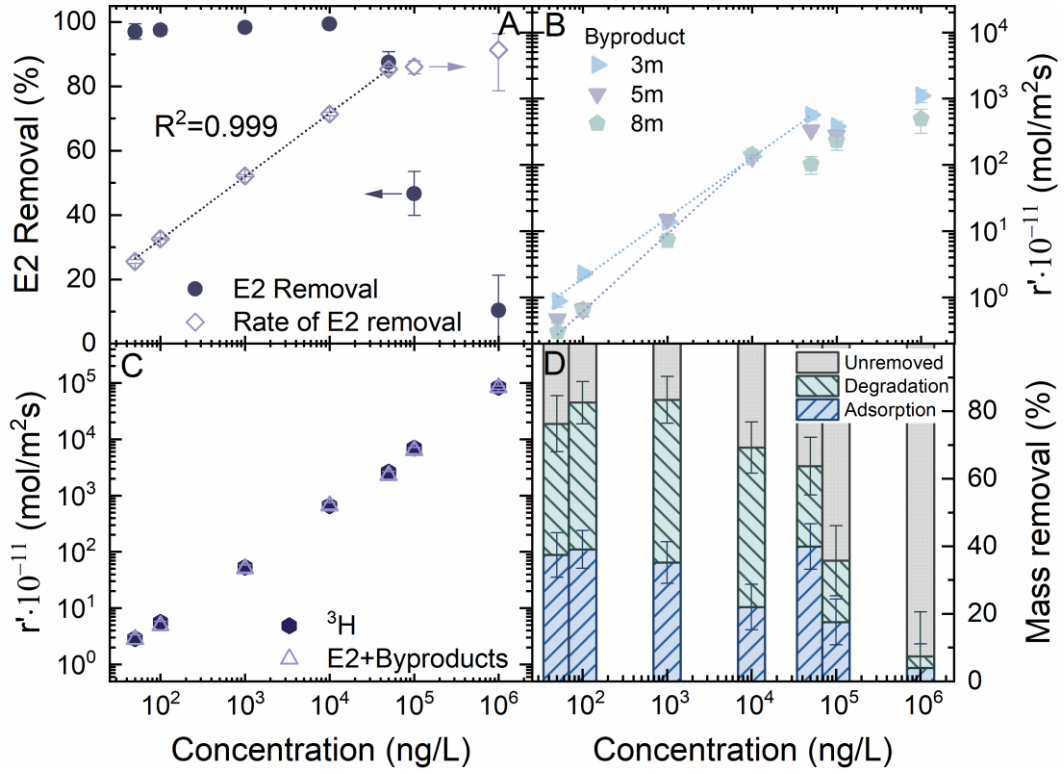

Figure 27. Impact of initial concentration on the electrochemical degradation of E2 expressed as (A) E2 removal and apparent rate of E2 removal, and (B) apparent rate of byproduct formation, (C) 3H, and the sum of E2 and the three byproducts in permeate; and (D) contribution to the mass removal of E2 by the electrochemical adsorption and degradation vs. temperature. $c_{f,E2}$ = 100 ng/L, V_{cell} = 1.6 V, J_f = 600 L/m2h (2 mL/min), 1 mM NaHCO3, 10 mM NaCl, 27.2 mg/L EtOH, 79.2 mg/L MeOH, pH 8.2±0.2. 23±0.2 ℃. Reprinted from [4].

Figure 27A reveals a clear linear relationship (R^2 = 0.999) between the apparent rate of E2 removal and its initial concentration, covering a range from 50 to $5 \cdot 10^4$ ng/L, before reaching a plateau at concentrations above $5 \cdot 10^4$ ng/L. This behavior suggests a reaction regime that is limited by the availability of E2 molecules at the membrane surface for concentrations between 50 and $5 \cdot 10^4$ ng/L. Remarkably, the removal rate plateaus at a maximum of $(3.8 \pm 2.9) \cdot 10^{-9}$ mol/m^{2}s once the E2 concentration exceeds $5 \cdot 10^4$ ng/L. This pronounced change signifies a shift from a concentration-limited

regime to one dictated by surface area availability, indicating that the reactive sites on the membrane interface become saturated with adsorbed E2 molecules.

3) Degradation mechanisms (heterogeneous *vs.* homogeneous) within the electrochemical and photocatalytic membrane processes

To elucidate the degradation mechanisms of SH within the CNT EMR, the principal reactive species involved, notably hydroxyl radicals (·OH [8, 9]) and active chlorine ([10, 11]), were identified across a range of cell voltages from 0.9 to 3V (Figure 28).

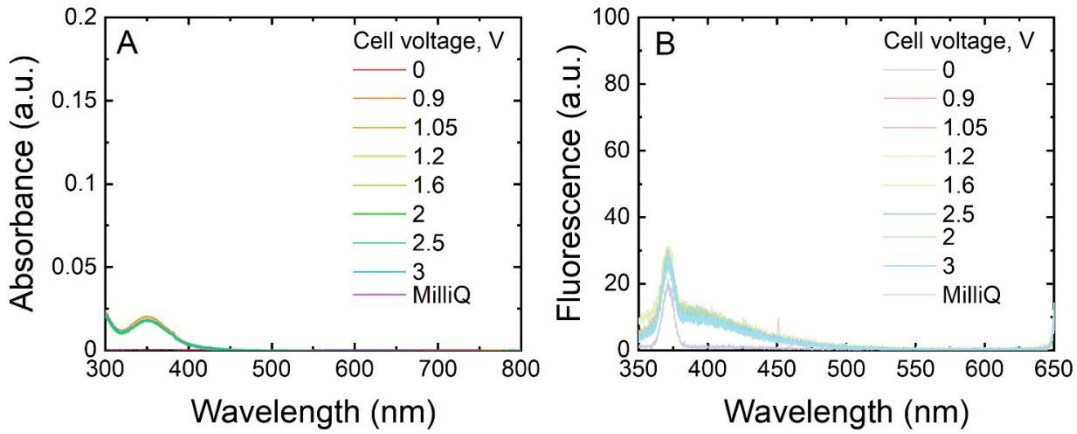

Figure 28. (A) Absorbance spectra of active chlorine in the permeate sample for filtration of a KI/NaAc/HAc solution at varying cell voltage from 0.9 to 3 V within the CNT EMR, and (B) fluorescence spectra of ·OH adduct in permeate for electrochemical filtration with 200 mL of coumarin solution at varying cell voltage from 0.9 to 3 V within the CNT EMR. $c_f(coumarin)$ = 0.01 mM, J_f = 600 L/m2h (2 mL/min), 10 mM NaCl, 1 mM NaHCO3, 27.2 mg/L EtOH, 79.2 mg/L MeOH, pH 8.3±0.3, 23±0.2 ℃. Reprinted from [4].

Figure 28A reveals that the absorbance at 352 nm for the permeate sample, across a range of applied voltages, matches that of the blank sample. This suggests that no measurable active chlorine was produced in the EMR, even under voltages as high as 20 V. The fluorescence spectra (Figure 28B) exhibited two features associated with water scattering and coumarin, yet no peaks corresponding to ·OH-coumarin byproducts were detected. This indicates that no significant ·OH radicals were generated by the CNT membrane under the tested conditions. These findings lead to the inference that direct electron transfer plays a central role in the degradation of SH, supported by fundamental electrochemical studies on the CNT membrane, which included cyclic voltammetry (CV) measurements (Figure 29).

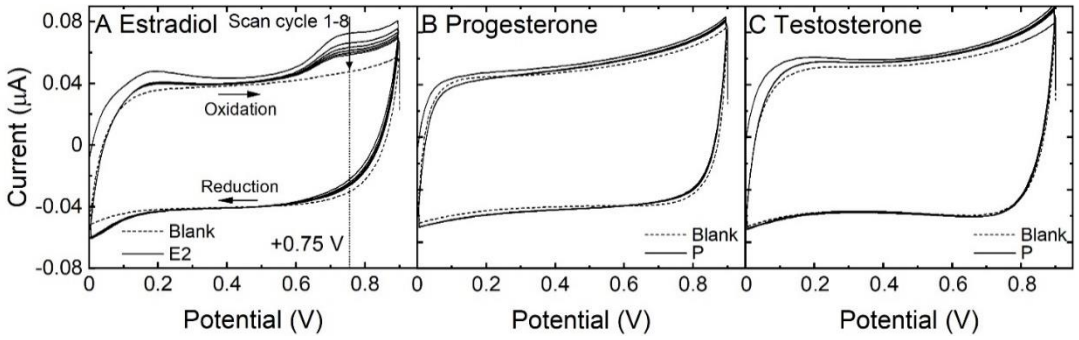

Figure 29. Cyclic voltammograms for 1 mg/L (A) estradiol, (B) progesterone, and (C) testosterone in electrolyte containing 10 mM NaCl, 1 mM $NaHCO_3$, 27.2 mg/L EtOH, and 79.2 mg/L MeOH in potentential range from 0 to 0.9 V with a scan rate of 100 mV/s. Reprinted from [4].

An anodic oxidation peak for E2 was identified at a potential of +0.75 V (*vs.* Ag/AgCl), with no discernible reduction peak in the reverse scan (Figure 29A). This observation points to the irreversible electrooxidation of E2 through direct electron transfer on the CNT membrane. Direct electron transfer is postulated to engage E2 in the liberation of two protons, leading to the formation of a phenoxy radical. This radical is capable of resonance within the aromatic ring, eventually transforming into a ketone derivative [12-14]. Such a chemical modification significantly alters the estrogenic activity of E2, primarily through changes to its phenolic binding group [15, 16]. The continued oxidation of E2 is anticipated to yield lower molecular weight compounds, potentially culminating in its complete mineralization to CO2.

To confirm the hypothesis of electron transfer mechanism in the E2 degradation within the CNT EMR, $NaNO_3$ was employed as a scavenger to target surface electrons (Figure 30).

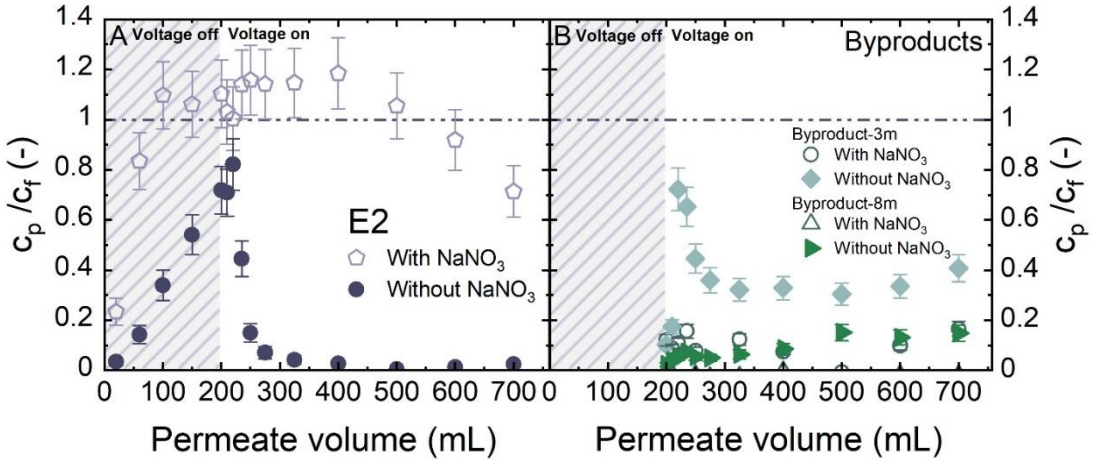

Figure 30. Electrochemical degradation of E2 in the presence of scavenger NaNO3 for surface electrons within the CNT EMR, as normalized concentration of (A) E2 and,

and (B) byproducts, vs. accumulated permeate volume. $c_{f,E2}$ = 100 ng/L, $c_{f,NaNO_3}$ = 10 mM, V_{cell} = 1.6 V, J_f = 600 L/m²h (2 mL/min), 1 mM $NaHCO_3$, 10 mM NaCl, 27.2 mg/L EtOH, 79.2 mg/L MeOH, pH 8.2±0.2, 23±0.2 ℃. Reprinted from [4].

The addition of 10 mM $NaNO_3$ notably hindered the removal of E2 in the CNT EMR, resulting in only minimal production of the degradation byproduct-3m. This outcome suggests that direct electron transfer is the dominant mechanism driving E2 degradation in the EMR.

To determine the contribution of different reactive species to the photocatalytic degradation of E2, the experiments were conducted with 1 and 10 mM of various scavengers (Figure 31).

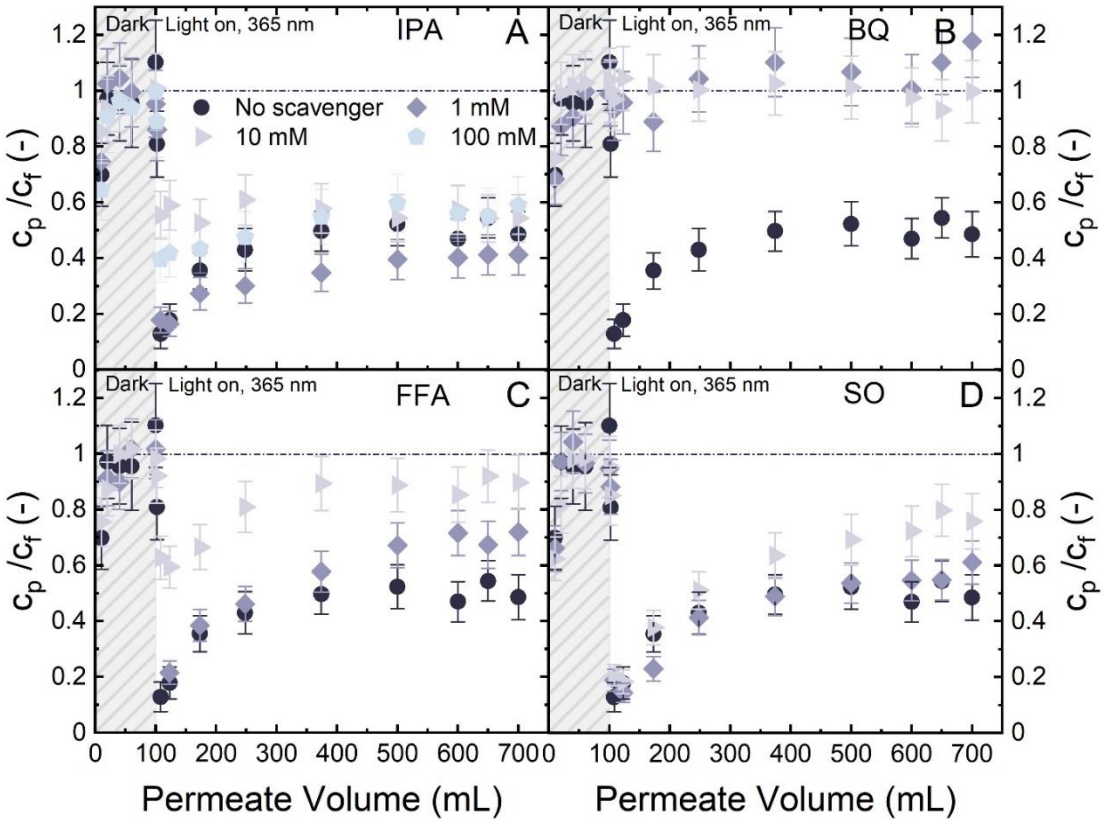

Figure 31. Effect of 1 and 10 mM (A) IPA, (B) BQ, (C) FFA, and (D) SO on the photocatalytic degradation of E2 (0.003 mM) expressed as normalized permeate concentration of E2 ($c_{p,E2}$ /$c_{f,E2}$) vs. cumulative permeate volume (V_p). PES-TiO2, $c_f(E2)$ = 100 ng/L, I_{inc} = 10 mW/cm2, 365 nm, J_f= 600 L/m2h, 1 mM NaHCO3, 10 mM NaCl, 27.2 mg/L EtOH (0.3 mM), 79.2 mg/L MeOH (2.5 mM), pH 8.3±0.3, 23±0.2 ℃. Data adapted from [17].

The presence of either 1 or 10 mM IPA did not significantly impact the degradation of E2 in the PMR system, suggesting that ·OH did not play a role in the degradation process. This lack of effect may be attributed to the scavenging action of the buffer

solution components—ethanol, methanol, and $NaHCO_3$—on the ·OH radicals. Conversely, the introduction of either 1 or 10 mM BQ completely halted E2 removal. BQ is known to react with both $\cdot O_2^-$ and ·OH, but given that IPA, a known ·OH scavenger, did not influence E2 degradation, it's logical to deduce that $\cdot O_2^-$ is the primary ROS responsible for E2 removal in the PMR system.

The E2 removal dropped from 47±8% to 26±8% and 7±9% with the addition of 1 and 10 mM FFA, respectively. FFA can interact with both $^1O_2$ and ·OH. However, the reduction in E2 removal, despite the presence of FFA, underscores that while $^1O_2$ may contribute to E2 degradation, its role is significantly less critical compared to $\cdot O_2^-$. An alternative explanation could be that FFA scavenges a minor fraction of $\cdot O_2^-$ [18], thus diminishing E2 removal efficiency. No discernible impact was observed with SO, which suggests that valence band holes (h_{VB}^+) either do not contribute or contribute minimally to E2 degradation.

Reference

[1] R. Lyubimenko, B.S. Richards, A. Turshatov, A.I. Schäfer, Separation and degradation detection of nanogram-per-litre concentrations of radiolabelled steroid hormones using combined liquid chromatography and flow scintillation analysis, Scientific Reports, 10 (2020) 7095

[2] X. Zhu, A.V. Dudchenko, C.M. Khor, X. He, G.Z. Ramon, D. Jassby, Field-induced redistribution of surfactants at the oil/water interface reduces membrane fouling on electrically conducting carbon nanotube UF membranes, Environmental Science & Technology, 52 (2018) 11591-11600

[3] D. Jassby, M. Wiesner, C.-f. De Lannnoy, Electrically conducting reverse osmosis membranes, in, U.S. Patent 9,802,163, Issued October 31, 2017.

[4] D.J. Siqi Liu, Andrea I. Schäfer, Removal of steroid hormone in a carbon nanotube electrochemical membrane reactor: Adsorption, degradation, and formation of metabolites, (2024)

[5] CF016A electrode modified crossflow assembly, acrylic, in, https://www.sterlitech.com/cf016a-electrode-modified-crossflow-assembly-acrylic.html.

[6] S.L.D.J.D.M.A.I. Schäfer, Removal of steroid hormone micropollutants by electrochemical carbon nanotubes membrane in a flow-through reactor: Differentiation between electrochemical adsorption and degradation, (2024)

[7] S. Lotfi, K. Fischer, A. Schulze, A.I. Schäfer, Photocatalytic degradation of steroid hormone micropollutants by TiO_2-coated polyethersulfone membranes in a continuous flow-through process, Nature Nanotechnology, 17 (2022) 417-423

[8] K. Jiang, S. Back, A.J. Akey, C. Xia, Y. Hu, W. Liang, D. Schaak, E. Stavitski, J.K. Nørskov, S. Siahrostami, H. Wang, Highly selective oxygen reduction to hydrogen

peroxide on transition metal single atom coordination, Nature Communications, 10 (2019) 3997
[9] H. Liu, C.D. Vecitis, Reactive transport mechanism for organic oxidation during electrochemical filtration: Mass-transfer, physical adsorption, and electron-transfer, Journal of Physical Chemistry C, 116 (2012) 374-383
[10] W.-L. Wang, Q.-Y. Wu, N. Huang, T. Wang, H.-Y. Hu, Synergistic effect between UV and chlorine (UV/chlorine) on the degradation of carbamazepine: Influence factors and radical species, Water Research, 98 (2016) 190-198
[11] E. Brillas, I. Sirés, Electrochemical remediation technologies for waters contaminated by pharmaceutical residues, in: E. Lichtfouse, J. Schwarzbauer, D. Robert (Eds.) Environmental Chemistry for a Sustainable World: Volume 2: Remediation of Air and Water Pollution, Springer Netherlands, Dordrecht, 2012, pp. 297-346.
[12] M.M. Ngundi, O.A. Sadik, T. Yamaguchi, S.-i. Suye, First comparative reaction mechanisms of β-estradiol and selected environmental hormones in a redox environment, Electrochemistry Communications, 5 (2003) 61-67
[13] Y. Ohko, K.-i. Iuchi, C. Niwa, T. Tatsuma, T. Nakashima, T. Iguchi, Y. Kubota, A. Fujishima, 17β-estradiol degradation by TiO_2 photocatalysis as a means of reducing estrogenic activity, Environmental Science & Technology, 36 (2002) 4175-4181
[14] J. Mai, W. Sun, L. Xiong, Y. Liu, J. Ni, Titanium dioxide mediated photocatalytic degradation of 17β-estradiol in aqueous solution, Chemosphere, 73 (2008) 600-606
[15] Y. Zhao, J. Hu, W. Jin, Transformation of oxidation products and reduction of estrogenic activity of 17β-estradiol by a heterogeneous photo-Fenton reaction, Environmental Science & Technology, 42 (2008) 5277-5284
[16] A.M. Brzozowski, A.C.W. Pike, Z. Dauter, R.E. Hubbard, T. Bonn, O. Engström, L. Öhman, G.L. Greene, J.-Å. Gustafsson, M. Carlquist, Molecular basis of agonism and antagonism in the oestrogen receptor, Nature, 389 (1997) 753-758
[17] S. Liu, P.C. Edara, A.I. Schäfer, Influence of organic matter on the photocatalytic degradation of steroid hormones by TiO_2-coated polyethersulfone microfiltration membrane, Water Research, 245 (2023) 120438
[18] Y. Guo, J. Long, J. Huang, G. Yu, Y. Wang, Can the commonly used quenching method really evaluate the role of reactive oxygen species in pollutant abatement during catalytic ozonation?, Water Res, 215 (2022) 118275

2. CONCLUSIONS

Despite the difficulties in the pandemic, the Israeli and German group have collaborated closely and finalized most of the proposed tasks of the project. This project integrated nanotechnologies with electrochemical reactions in a composite membrane to achieve in-situ monitoring of micropollutants (MPs) in polluted or reused (treated) water, and remove micropollutants effectively in water reuse. The main outcomes of includes:

i) The efficiency of homogeneous and heterogeneous Fenton-like oxidation processes in removing propoxur (PR) was investigated in a submerged ceramic membrane

reactor operated in a continuous mode. A freshly prepared amorphous heterogeneous catalyst was synthesized and characterized, revealing a layered porous structure of 5–16 nm nanoparticles that formed aggregates (33–49 µm) known as ferrihydrite (Fh). The membrane exhibited a rejection of >99.6% for Fh. The homogeneous catalysis (Fe^{3+}) exhibited better catalytic activity than the Fh in terms of PR removal efficiencies.

ii) A novel electrochemical membrane cell was developed for both monitoring and removing MPs, including 4-NP, CBZ, and PFAS, from reused water. Several configurations of larger flow-through electrochemical cells were created, including a 3D-printed version. The faradaic efficiencies for the formation of H_2O_2 and ·OH were assessed using various carbon-based electrodes, such as carbon felt, carbon sponge, and CNTs. The results indicated that the faradaic efficiency for H_2O_2 reduction was exceptionally high when CNTs coated with a porphyrin catalyst were used, although the oxygen reduction reaction (ORR) displayed low efficiency in generating ·OH radicals.

iii) The electrochemical degradation of SHs using an ultrafiltration membrane immobilized with CNTs in a single-pass flow-through EMR was investigated at environmentally realistic concentrations (50 – 10^6 ng/L). The CNT EMR demonstrated high efficiency in eliminating E2 from a feed solution of 100 ng/L, utilizing a cell voltage of 1.6 V and a water flux of 600 L/m²h·bar (flow rate 2 mL/min), which achieved a permeate concentration below the detection limit (2.5 ng/L) after treatment. Direct electron transfer was identified as the primary mechanism driving the degradation of SHs in the CNT EMR, whereas superoxide radicals was found to dominate the mechanisms of MP degradation in a photocatalytic membrane.

These results highlight the significant potential of integrating nanotechnologies into electrochemical membrane processes for monitoring MPs and reusing water. Building on these achievements, the Israeli group from HUJI and the German group from the KIT have submitted a joint proposal for funding through the BMBF-MOST program to scale up the application of this electrochemical membrane process for agricultural wastewater reuse.

3. PUBLICATIONS, PATENTS, INVENTIONS:

- Abed-Alhakeem Azaiza, Raphael Semiat, Hilla Shemer. Competitive Study of Homogeneous and Heterogeneous Fenton-like Flow-through Propoxur Oxidation in ROC Solution. Water Science & Technology 87(11), 2023, 2890–2904.
- Siqi Liu, Pattabhiramayya C. Edara, Andrea I. Schäfer*. Influence of organic matter on the photocatalytic degradation of steroid hormones by TiO_2-coated polyethersulfone microfiltration membrane. Water Research, (2023) 245: 120438.
- Siqi Liu, Eléonore Véron, Shabnam Lotfi, Kristina Fischer, Agnes Schulze, Andrea I. Schäfer*. Poly(vinylidene fluoride) membrane with immobilized TiO_2 for degradation of steroid hormone micropollutants in a photocatalytic membrane reactor. Journal of Hazardous Materials, (2023) 447:130832.
- Siqi Liu, David Jassby, Daniel Mandler, Andrea I. Schäfer*. Removal of steroid hormone micropollutants by electrochemical carbon nanotubes membrane in a flow-through reactor: Differentiation between electrochemical adsorption and degradation. (2024) Submitted.
- Siqi Liu, David Jassby, Andrea I. Schäfer* Removal of steroid hormone in a carbon nanotube electrochemical membrane reactor: Adsorption, degradation, and formation of metabolites. (2024) In preparation.